

# **Selective leaching studies of sediments from a seamount flank in the Central Indian Basin: Resolving hydrothermal, volcanogenic and terrigenous components using major, trace and rare-earth elements**

**M. B. L. Mascarenhas-Pereira\* & B. Nagender Nath**

Geological Oceanography Division, National Institute of Oceanography,  
Dona Paula, Goa, 403004, India

\*corresponding author: Fax: 91-832-2450602 [mariab@nio.org](mailto:mariab@nio.org)

## **Abstract**

We have investigated the sediments from a site where a newly discovered submarine hydrothermal alteration of recent origin is located to identify the source components and estimate their relative contribution. The site is situated on the flank of a seamount in the Central Indian Basin along the 76° 30' E fracture zone which traces the movement of the Rodriguez triple junction. Detailed analyses of major, trace and rare earth elements (REE) on the bulk, leach, residue and clay fraction, and infra red spectroscopy studies of the clay fraction helped characterize the hydrothermal nature of the sediments. Selective dissolution carried out using HCl has allowed the discrimination between a leach phase (leachable Fe-Mn oxide) and a residue phase (refractory). The sediments are iron-rich, majority of Fe, Mn is in leachable fraction and are compositionally comparable to ridge-crest metalliferous sediments. Elemental ratios and geochemical discrimination plots of major element data reveal that the sediments are a mixture of Fe-rich mineral phases on one hand apparently from hydrothermal sources and aluminosilicates such as illite, zeolites, micaceous clays and smectites contributed from the Bengal fan, weathering of basinal basalts and authigenic processes. Ternary mixing calculations of bulk sediment

major element data show that 35-45 % metalliferous sediments could reproduce Fe and Mn values of our sediments.

The shale normalized REE patterns of the bulk sediments are remarkably similar to those of the HCl soluble leach fraction, implying that the REEs in the HCl soluble leach fraction dominate the bulk fraction. HCl leachates exhibit characteristics of vent fluids as well as seawater with pronounced Eu anomaly with HREE enrichment and negative Ce anomaly. The residue on the other hand has a high concentration of Fe, V, Zn, and Pb indicating a sulfidic input to the sediments. Ternary mixing calculations of REEs carried out on the residual fraction indicate that the sulfide-like material dominates (64–72 %) over terrigenous (10–20 %) and MORB derived (16–18 %) components.

This study helped us identify and quantify two types of hydrothermal material in the sediments, dominated by Fe-Mn phases (ferruginous oxides and silicates; Mn-oxides) in leachable fraction and sulfide-like material in residual phases. The clay fraction is mainly composed of dioctahedral smectites and has a composition similar to Alvin nontronite. The geochemical and mineralogical characteristics collectively suggest that these sediment-hosted precipitates formed at relatively low temperatures ranging between 50 and 100° C from a mixture of seawater and hydrothermal fluids.

The presence of hydrothermal sediments in the vicinity of a fracture zone suggests the occurrence of localized hydrothermal activity associated with intra plate volcanism. This is probably induced by reactivation of tectonic forces along the fracture zones.

## **1. Introduction**

Submarine hydrothermal activity is a widespread feature occurring in all the oceans along the spreading centers at mid oceanic ridges and at subduction areas. Most of the sites discovered in the Indian Ocean so far are located along the mid-oceanic ridge system with some at the Andaman back arc basin (Banerjee and Ray, 2003; Gallant and Von Damm, 2006; Bach et al., 2002; Kurian et al., 2008). In addition to the spreading centers, hydrothermal activity can also occur in oceanic seamount areas. Intraplate seamounts are produced from the upwelling of “small plumes” which transport lower mantle material underneath the ridge axis. The leaking of this lower mantle material gives rise to axial and off axial volcanism (Hékinian et al., 1999). Hydrothermal deposits at intraplate seamounts are less common,

although the seamount morphology associated fracturing and volcanism could favor hydrothermalism (Alt, 1988). Such seamounts have been reported from the Pacific viz., Macdonald, Loihi (Karl et al., 1988), Vailulu'u (Staudigel et al., 2004). Signatures of the hydrothermal nature of the Central Indian Basin (CIB) sediments were only reported through microscopic spherules (see Iyer, 2005 and references therein). Native aluminum-rich particles of hydrothermal origin (Iyer et al., 2007), volcanic glass associated with pumice and palagonites (Mascarenhas-Pereira et al., 2006) was recovered from the sediments located on the flank of a seamount along the 76° 30' E Fracture zone in the CIB and indicated the occurrence of intraplate submarine volcanism and hydrothermal activity. Recent isotopic studies ( $^{210}\text{Pb}$ ,  $^{10}\text{Be}$  and  $^{230}\text{Th}$ ) on the sediments from the same area have revealed hydrothermal alteration of sediments of recent origin through ascending fluid flow (Nath et al., 2008).

In this study, we have employed major, trace and rare-earth element (REE) geochemistry (along with other elements) to characterize the different source components and to estimate their relative contribution to the sediments from the flank of a seamount along the fracture zone. We have extracted the hydrothermal component in the sediments by selective leaching using 50% HCl. The chemistry of hydrothermal component in these sediments allowed a comparison with previously published geochemical data of hydrothermal material from other major spreading centers (Rainbow, TAG, MAR and EPR). Bulk and leach data was used for mixing calculation to find the proportion of the different source components. Based on these studies, we report the occurrence of sediments of distinctly metalliferous nature with ferruginous smectites and nontronite at this intraplate seamount setting. This is the first report of hydrothermal signatures being imprinted on the bulk chemistry of the sediments in an intraplate region of the CIB.

## **2. Regional setting and hydrothermalism**

The CIB is bounded by the Ninety East ridge, the Central Indian ridge and the Southeast Indian ridge, and is between 50–60 Ma in age (Mukhopadhyay and Batiza, 1994). There exists three major fracture zones that trend along 73° E (Vishnu or La Boussole), 76° 30' E and 79° E (Indrani or L'Astrolabe) and the Triple Junction Trace on the Indian Plate (TJT-In) between 76–78° E longitude (Kamesh Raju and Ramprasad, 1989). The sediment core studied here is recovered from the southern end of the 76° 30' E fracture zone (Fig. 1b) which represents the trace of Indian Ocean Triple Junction movement (Kamesh Raju and Ramprasad, 1989; Kamesh Raju, 1993). This is one of the six N–S

fracture zones represented in the CIB (Kamesh Raju, 1993, and references therein). Several seamounts were delineated along the fracture zones in the CIB, with the majority clustering along 76° 30' E and 79° E fracture zones (Fig. 1b). Clustering of seamounts along the fracture zones as seen here, is similar to non-hotspot volcanoes in the Pacific (Das et al., 2007), which preferentially occur either on or very near to the fracture zone. The fracture zones may provide easy conduits for formation of seamounts (Batiza, 1982). There may also be local perturbations to the plumbing system or other zones of weakness that control the location of seamounts (Epp and Smooth, 1989; Kamesh Raju, 1993). Such local perturbations to the plumbing system possibly from tectonic reactivation of the fracture zones may be responsible for the intraplate volcanism and the hydrothermal activity metalliferous sediments in this area.

Possibility of intraplate volcanism and the associated hydrothermal activity in CIB has been reported in the past. Occurrence of volcanic spherules, glass shards (Gupta, 1988; Iyer et al., 1997; Mascarenhas-Pereira et al., 2006; Nath and Rao, 1998; Sukumaran et al., 1999); volcanogenic-hydrothermal material consisting of Fe-Si oxyhydroxides, volcanic spherules, glass shards, ochrous metalliferous sediments and spherules (Iyer et al., 1997), spillites in the vicinity of 79° E fracture zone (Karisiddaiah and Iyer, 1992), zeolitites (Iyer and Sudhakar, 1993), fossil free smectite-rich pyroclastic layers at different subsurface depths representing episodic volcanic activity (Nath and Rao, 1998) in CIB were reported in the past. In a recent study by Iyer et al. (2007), native aluminium of submarine hydrothermal origin was reported from the core AAS 61/BC 8.

### **3. Sampling and analytical work**

A short sediment core AAS 61/BC 8 was collected using a large box corer (50 x 50 x 50 cm) at 16° S and 75° 30' E from the flanks of a seamount from the CIB along the southern end of the 76° 30' E fracture zone from a water depth of 5010 m (Fig. 1) during the 61<sup>st</sup> cruise of RVAA Sidorenko during the year 2003. The core was sampled from pelagic red clay sediment domain (see Nath et al., 1989 for sediment types in CIB). The core was sub sectioned into 2 cm intervals. Clays of < 2 µm size were separated using standard settling velocity technique.

Bulk samples along with clay samples were dissolved following acid dissolution procedure of Balaram and Rao (2003). The resulting solutions were analyzed for REE along with some trace and major elements by Inductively Coupled Plasma Mass Spectrometry (ICP-MS) at the National

Geophysical Research Institute, Hyderabad, India. 10 ml of acid mixture containing HF, HNO<sub>3</sub> and HClO<sub>4</sub> (in the ratio of 6:3:1) was added to ~ 50 mg of sample and USGS Marine mud standard MAG-1 in teflon beakers. The solutions were then evaporated to dryness in the fume hood. After 30 min, 2 ml of conc. HCl was added to remove any black particles, if present. The acid mixture was kept on sand bath till it was evaporated to dryness. 5 ml of 1 ppm Rh solution and 20 ml of 1:1 HNO<sub>3</sub> were added and made up to 250 ml and cooled. The clear solutions were then introduced into ICP-MS for elemental analysis.

Following the bulk analyses, selective chemical leaching was carried out using hot 50 % HCl on 4 sample intervals and USGS standard MAG-1 (following the technique described in Cronan, 1976). Accurately weighed representative subsamples of 1 gm each were leached with hot 50 % HCl and kept hot by continuous shaking in a heated water bath for 4 hours prior to filtration. The dissolved material was filtered through previously weighed filter papers and the residues were weighed. The leach solutions were analyzed by ICP-MS for the same elements as the bulk samples, using standards made up in the same solutions as the samples. The same leaching procedure (with hot 50 % HCl) was carried out on a different subsample (4 sediment sections) for major element analyses. MAG-1 was included during this batch of leaching. Bulk sediments and the residue left after leaching were analyzed for major elements using X-ray Fluorescence Spectroscopy (XRF) at NIO, Goa. Elemental data of Fe, Al and Mn are obtained by both ICP-MS (Table 1) and XRF methods (Table 2) for four subsections, The results of Fe and Al by both the methods agree well (< 11% variability), while the variability for Mn is relatively large probably due to inhomogeneity between the two subsamples used. It should also be mentioned here that the Mn values for MAG-1 obtained by both the methods concur well with the certified value (Tables 2 and 3). We prefer to use ICP-MS data for these 3 elements for interpretations as the data for entire core is available.

The leach was expected to contain amorphous Fe-Mn oxides, carbonate minerals and adsorbed trace elements, crystalline iron oxides, hydrothermal silicates, weathered detrital/clay phases and partially dissolves sulfide component if any (Cronan and Hodkinson, 1997). The residue, on the other hand, was expected to contain mainly the resistant silicates and aluminosilicates insoluble in HCl (detrital phase) and the sulfides if any. Though a large number of leaching techniques are available in the literature, acid based leaching with low pH are found to be suitable for elements like REE

(Sholkovitz, 1989; Nath et al., 1994). The leach used here has also been adopted elsewhere for assessing the hydrothermal component in sediments (Chavagnac et al., 2005).

Precision and accuracy of ICP–MS analyses carried out on MAG–1 in duplicate are presented in Table 3. Accuracy was better than 5 % for Al, Fe, La, Sm and U, while it was better than 2 % for all other elements. Data shows an excellent precision for all the elements studied here (better than 5 %: Table 3).

In order to know the recovery of material in the leaching experiment, we compared our results for MAG–1 (bulk and residue) with those of Kryc et al. (2003) (Table 4) who reported sequential extraction procedure for Si, Al, Ti, Fe, Ca, Mn P and Ba in five sedimentary reference materials. It should however be noted that the extraction procedures were different in both the studies. In general, there is a good agreement for all elements (except Fe and Mn) between the results of our study and those of Kryc et al. (2003) (Table 4) despite the difference in techniques and analytical methods adopted for the residual extraction. Our residues contained lower Fe and Mn than Kryc et al. (2003) probably in view of the stronger leach (hot 50 % HCl vis-à-vis the hydroxylamine hydrochloride used by Kryc et al., 2003) used by us.

Infrared spectroscopic studies were carried out on the <2 µm size clay fraction pellets (pressed with KBr powder) using a Shimadzu 8201 PC at the National Institute of Oceanography, Goa. Organic carbon measurements were made using wet oxidation method of El Wakeel and Riley (1957). The level of precision and accuracy routinely obtained in our laboratory are described in Nath et al. (1997a).

## **4. Results and Discussion**

Major and REE data for the bulk sediments is presented in Table 1 and 2 and those of leach and residues are shown in Table 5.

### **4.1. Lithological variation**

The sediments in the study area show two subsections (units) based on color. While the unit 1 (0–6 cm bsf) display a light brown color, unit 2 (6–20 cm bsf) exhibits a dark brown to black coloration. The coarse fraction (>63 µm) shows an abundance of radiolarians in unit 1, which gradually decreases in abundance, leading to complete absence in unit 2. The transition from pelagic to indurated sediment is

marked by the absence of radiolarians and the presence of ichthyoliths. Radiolarian dissolution features were clearly evident in SEM pictures of unit 2 sediments (Nath et al., 2008). Glass shards are present throughout the core, but are abundant in unit 2 (Mascarenhas–Pereira et al., 2006). Aluminium–rich grains of hydrothermal origin were recovered mainly from unit 2 (Iyer et al., 2007). Palagonitic grains were present throughout the core with colors ranging from white, yellow to brown and with a waxy luster. Biostratigraphy and radiometric dating has shown that the unit 1 is younger than 180 kyrs. (Mascarenhas–Pereira et al., 2006).

## **4.2 Identification of source**

### **4.2.1 Major element geochemistry and interpretation of mineral associations**

The major element composition of bulk and the residues are presented in Table 2. Two major features stand out. In general the sediments have low silica compared to CIB sediments (Nath et al., 1989) and high Fe content suggesting a ferruginous nature. Si/Al ratio in bulk sediments is ~2.8, which is less than that reported for typical quartz mineral/biogenic silica (>5, Ziegler et al., 2007), while the residue has a higher ratio of Si/Al (~ 4). This is consistent with the mineralogy of the core which has low siliceous skeletal remains with dissolution effects seen on some of the radiolarians (Mascarenhas–Pereira et al., 2006; Nath et al., 2008). However Fe/Si ratio of the bulk (0.35–0.48) is comparable to authigenic Fe rich smectites associated with hydrothermal process in other areas (Central Pacific, Ziegler et al., 2007; DOMES area in North Pacific, Hein et al., 1979). The Na/K ratio in leach residues range between 0.32 and 0.37 and closer to ~0.35 assigned to phillipsite (Kastner, 1979; Ziegler et al., 2007) and is consistent with the volcanogenic–hydrothermal content in unit 2 (Mascarenhas–Pereira et al., 2006; Iyer et al., 2007).

Unpublished X–ray diffraction studies have shown that the sediments contain a mixture of quartz, plagioclase feldspars, illite, alteration mineral smectite and authigenic silicate such as zeolites (mainly phillipsite). Earlier studies have shown that the CIB sediments contain illite, chlorite and kaolinite mainly derived from turbiditic currents from Ganges–Brahmaputra through Bengal fan (Rao and Nath, 1988; Debrabant et al., 1993), smectite derived from the weathering of basinal basaltic rocks; with presence of both Al– and Fe–rich montmorillonites (Rao and Nath, 1988). Phillipsite and clinoptilolite are major zeolitic minerals present in CIB sediments (V. P. Rao and B. N. Nath, unpublished data). In the following section on infra–red spectroscopy studies, we have also discussed

the presence of nontronite, ferruginous smectites and beidellites in these sediments. We have plotted two x–y scatter diagrams ( $\text{Al}_2\text{O}_3$  versus  $\text{Fe}_2\text{O}_3$  and  $\text{K}_2\text{O}$  versus  $\text{Al}_2\text{O}_3$ ), and one ternary diagram (K–A–CN) to infer the mineralogy (Figs. 2 and 3). Literature values of chemical composition for clay minerals (Kaolinite, smectite, illite and chlorite from Grim, 1968 and references therein), plagioclase, zeolites (Deer et al., 1967 and references therein).in addition to Al–Bediellite and nontronite (Aoki et al., 1996) and authigenic Fe–montmorillonite of hydrothermal origin (McMurtry and Yeh., 1981) are used as possible sources. In addition, chemical data on separated clays from the distal Bengal fan (Aoki et al., 1991) are also included.

In the  $\text{Al}_2\text{O}_3$  vs.  $\text{Fe}_2\text{O}_3$  plot (Fig. 2a), the bulk sediments fall in between Fe–rich fields of Fe–montmorillonites, nontronites and Bengal fan smectites on one side and Al–rich end members of smectite, beidellite, micaceous clays from Bengal fan, chlorite, zeolite and plagioclase on other. This could be accounted by the presence of a mixture of variable proportions of  $\text{Al}_2\text{O}_3$  supplied by illite, plagioclase, smectite and zeolites and  $\text{Fe}_2\text{O}_3$  contributed by nontronite and Fe–montmorillonite. The residue plot closer to the smectites and micaceous clays of Bengal Fan as compared to the bulk indicating the removal of Fe from the authigenically formed nontronites and Fe–montmorillonite from the bulk sediments. This is also manifested by the Fe/Al ratio of bulk ( $> 1.02$ ) being more than the residue ( $< 0.61$ ). The Fe/Al ratio of residue in the surface sediments approaches the value of PAAS ( $\sim 0.51$ ). The source composition mainly of aluminosilicate fraction is further constrained from the  $\text{K}_2\text{O}$  and  $\text{Al}_2\text{O}_3$  plot (Fig. 2b), wherein our sediment data plot between two trend lines, first defining illite, Bengal Fan micaceous clays and the other with overlapping compositional fields of plagioclase, smectite, chlorite, kaolinite, beidellite and zeolites. Thus, the aluminosilicates in these sediments may reflect the mixing of these two groups of mineral sources. The residue data fall close to bulk data with slight fall in K and Al values. Support also comes from the ternary diagram of  $\text{K}_2\text{O}$ – $\text{Al}_2\text{O}_3$  – ( $\text{CaO}+\text{Na}_2\text{O}$ ) (Fig. 3), where our bulk sediment data is sandwiched between fields defining zeolite, plagioclase and Fe–smectites on one side and illite, Al–rich beidellite, micaceous clays from Bengal Fan, kaolinite and chlorite on other. The bulk sediments exhibit a loss in  $\text{CaO}+\text{Na}_2\text{O}$  on leaching with hot 50 % HCl and a concomitant gain in  $\text{Al}_2\text{O}_3\%$ . The bulk sediments are apparently stripped off of CaO and  $\text{Na}_2\text{O}$  from the Fe–montmorillonite, phillipsite and plagioclase with the residue exhibiting compositional similarity with Bengal Fan smectites.



#### 4.2.1.1 Fe, Mn and minor element geochemical constraints on metalliferous/hydrothermal contribution

The Fe, Mn contents (Table 1) and Fe/Mn ratios (Table 6) correspond with those found in Central Indian ridge sediments and Fe oxides of hydrothermal origin from the EPR and north Fiji basin (Table 6, Plüger et al., 1986; Walter and Stoffers, 1985; McMurtry et al., 1991) implying the presence of a hydrothermal component in our sediments. The Fe/Mn ratios of our sediments are distinctly similar to ridge flank metalliferous sediments (Fig. 4). Mn concentrations in residues are < 2% of the bulk concentrations indicating that it occurs predominantly in the oxide/oxyhydroxide form. Assuming that majority Mn is of non-crustal origin, excess Fe/Mn (over the crustal ratio) is higher in unit 2 compared to unit 1, indicating a higher hydrothermal component in unit 2 sediments. Iron is present in a significant amount in the fraction soluble in HCl (~86 %). Studies have shown that Fe from minerals like goethite and clay minerals of the smectite group can be stripped by HCl attack. Therefore the relatively high iron content in the HCl soluble phase indicates the high concentration of non-detrital iron bearing minerals. In a ternary plot of Al-Fe-Mn, our bulk data fall in the field of Bauer deep metalliferous sediments (Fig. 5).

The “Metalliferous sediment index”  $100 \cdot \text{Al}/(\text{Al}+\text{Fe}+\text{Mn})$  values (MSI, based on Boström and Peterson, 1969; Table 6) is higher than those found in Kairei (26–32 %; German, 2003) and Rainbow hydrothermal fields (23–26 %; Cave et al., 2002) likely due to the presence of “Al-rich” lithic grains of hydrothermal origin in the sediments (Iyer et al., 2007). MSI values are lower in unit 2 suggesting that the metalliferous sediment component is relatively higher in unit 2 sediments.

In all the samples, cobalt, nickel and copper are predominantly present in the HCl soluble phase (up to 98 %). In addition, elements like Fe, V, Pb are also principally associated with the non detrital phase (Table 5). Such a combination of elements has been termed as “hydrothermally associated elements” by Cronan and Hodkinson (1997).

We have used Co/Zn ratios to discriminate the sources of Fe-Mn oxides, similar to that adopted for Fe-Mn oxides (e.g., Toth, 1980; Nath et al., 1997b), considering that Co is a typical hydrogenous element enriched in hydrogenous precipitates scavenged from seawater while, Zn can be derived from a hydrothermal source. Analytical data on bulk sediments (AAS 61/ BC 8 core) studied here shows that the Co/Zn ratio (0.70 to 0.83, Table 6) falls close to the value for Fe-Mn oxides of mixed hydrothermal

hydrogenous origin from the Rodriguez Triple Junction (RTJ) in the Indian Ocean (Nath et al., 1997a). In a scatter plot (Fig. 6) of Co+Ni+Cu versus Co/Zn (following Toth, 1980), Co+Ni+Cu values of bulk sediments lie between 500 to 1500 ppm and plot very close to the hydrothermal–hydrogenetic boundary line (Fig. 6, modified from Nath et al., 1997a). Although Co/Zn in bulk sediments is almost similar in both the units, the HCl soluble leach phase is clearly differentiated with sediment depth. Data for the HCl leachates of unit 1 (4–6 cm and 8–10 cm) plot away from the hydrothermal–hydrogenetic fields with Co/Zn values between 9 and 12, while those of unit 2 (12–14 cm and 18–20 cm) lie closer to the hydrothermal–hydrogenetic boundary. This is consistent with the variable hydrothermal component in the two units.

Zn/Fe ratios (~ 0.0024 obtained here) are comparable to hydrothermal Fe oxides from the north Fiji basin (Table 7, McMurtry et al., 1991), Fe–Mn oxides of EPR (Walter and Stoffers, 1985), as well as CIR sediments (Plüger et al., 1986). Relative proportion of zinc is higher compared to Cu in residues (Table 5). Hydrothermal precipitates are generally characterized by relatively low Cu but high Zn concentrations (Kastner 1981). Massive sulfides analyzed from Mt. Jourdanne located on SWIR also show such association (Münch et al., 2001). The presence of high Zn (31%–80% of total Zn) in the residue may indicate the presence of sphalerite. The low concentration of Fe along with high Zn content in residue indicates Fe–poor sphalerite formed at temperature below 200 °C (Münch et al., 2001).

CIB sediments in pelagic red clay domain contain 2000–3000 ppm of Ba (Nath et al., 1989) compared to 463 to 732 ppm found in the core under consideration, which is almost 5 times lower than the surrounding sediments. This is consistent with depletion in biologically derived material viz., low organic matter and intense radiolarian dissolution in our core (Nath et al., 2008). Biologically derived barite grains were retrieved and studied earlier from CIB (Fagel et al., 1997). Considering a low biogenic contribution to the core studied here, barium could be from volcanogenic or hydrothermal sources. The values are closer to those found in hydrothermal sediments. For example, similar Ba concentration (550–571 ppm) were also observed in bulk hydrothermal sediments collected from the ODP site 834 and 835 in the Lau basin, SW Pacific (Cronan and Hodkinson 1997). Ba in the form of barite is a common precipitate from hydrothermal solutions (Dymond, 1981). We have analyzed Ba only in the bulk and thus unable to estimate the presence of barite in the residual phase.

#### 4.2.2. Mixing calculations using major element data of bulk sediments

Based on the possible source components interpreted from above discussion, relative proportion of each end member contributing to the bulk is assessed using ternary mixing equation with mass balance equation (Albarède, 1995; Chavagnac et al., 2005) shown below.

$$\int_{terrigenous} + \int_{metalliferous} + \int_{MORB} = 1$$

$$C_{mix}^i = (\int_{terrigenous} \times C_{terrigenous}^i) + (\int_{metalliferous} \times C_{metalliferous}^i) + (\int_{MORB} \times C_{MORB}^i)$$

where  $f$  represents the proportion of each end-member contributing to the bulk sediments and  $C_{mix}^i$  is the concentration of element  $i$  in the mixture of 3 end members. The end members used are metalliferous sediments from Bauer depression (Sayles and Bischoff., 1973), Indian MORB (Sun et al., 1979) and terrigenous sediments (Nath et al., 1989) from northern Indian Ocean (i.e. terrigenous material, metalliferous sediments and, MORB). The mixing calculations show that 35–45 % metalliferous sediments could reproduce Fe and Mn values of our sediments. Mixing calculations for other major elements such as Na and Mg also show affinity towards composition of metalliferous sediments, while the MORB contribution is apparently higher to Ti and Al.

#### 4.2.3. REE geochemistry

The behavior of the REE in high temperature seafloor hydrothermal fluids is well characterized (Michard and Albarède, 1986; Mitra et al., 1994). The REE concentrations are enhanced 10–10,000 times over sea water, due to extensive scavenging results in the net removal of these elements from the sea water (German et al., 1990). Based on REE studies on plume particles from EPR (comparing to that of TAG data of German et al., 1990), Sherrell et al. (1999) have shown that (i) the REE fractionation in hydrothermal systems varies over small ranges in each plume, (ii) the middle REE increase linearly with decreasing particulate Fe, (iii) the REE component reflect the mixing of primary hydrothermal precipitates with that of local resuspended material, (iv) the dissolved REE draw down occurs when the particulate Fe content is high (v) continued uptake of REEs by resuspended sediments takes place on at the surface and (vi) the Mn-oxides are not important carrier phases of REE (vis-à-vis Fe which is the prime carrier phase). The distinctive hydrothermal REE pattern of the near field sulfides and oxides is

therefore overprinted in metalliferous sediments, which have REE patterns characteristic of seawater (Barrett and Jarvis, 1988).

In this section, we discuss the REE geochemistry of bulk sediments as well as leach and residues of our samples in the light of published literature on plume particles and metalliferous sediments.

#### **4.2.3.1 REE content in bulk sediments**

REE content range between 526–607 ppm with relatively higher concentration in unit 1 compared to unit 2 (Table 6). The concentrations reported here are higher than those reported for the ridge–flank metalliferous sediments from the EPR (upto 300 ppm, Owen and Olivarez, 1988) and fall in the range of Leg 92 metalliferous sediments concentration (Barrett and Jarvis, 1988).

Post Archaen Australian Shale (PAAS; Taylor and McLennan, 1985) normalized patterns of bulk sediments studied here deviate markedly from a flat pattern (Fig. 7g), with the REE patterns of all the samples showing light REE (LREE) depletion. Uniformity in the REE patterns suggests either that the sediments are derived from a fairly homogeneous source (or sources) with respect to the REE, or may indicate mixing within the sediments (McLennan, 1989).

$(La/Yb)_n = (La/Yb)_{sample} / (La/Yb)_{PAAS}$ , which is an indicator of light to heavy REE fractionation, varies from ~0.46 for unit 1 to as much as 0.55 for unit 2 sediments (Table 6), indicating significant downcore HREE enrichment. HREE enrichment (e.g. low  $Nd_n/Yb_n$ : 0.56 and 0.59 and  $La_n/Yb_n$ : 0.46 to 0.55) together with low trace element concentration are indicative of low temperature fluids (Hodkinson et al., 1994; Mills et al., 2001). In contrast high temperature hydrothermal deposits have  $Nd_n/Yb_n$  values significantly above 1 (Mills and Elderfield, 1995; Frank et al., 2006).

Further corroboration of a metalliferous nature of the sediments comes from a binary plot of Cu+Ni+Co concentrations v/s  $\Sigma REE$  (Clauer et al., 1984), with the bulk and the HCl leach, representing the non–lithogenic component falling in the same field defined as metalliferous sediments (Fig. 8).

##### **4.2.3.1.1 Ce anomaly**

A significant feature of the REE patterns is the presence of negative Ce anomalies, with  $Ce/Ce^*$  ( $Ce^*$  obtained by linear interpolation between shale normalized La and Pr) values ranging from 0.66 to

0.79 with an average of 0.73 (Table 6), in contrast to the sediments overlain by nodules (Nath et al., 1992a) and typical hydrogenetic Fe–Mn oxides from the basinal parts of the Indian Ocean which all have positive Ce anomalies (Nath et al., 1992a, 1994; Nath, 1993). A negative Ce anomaly suggests a seawater source for the REEs, scavenged by Fe–oxyhydroxides (German et al., 1990; Sherrell et al., 1999). Previous work on metalliferous sediments has revealed shale–normalized patterns similar to our sediments with negative Ce anomaly and HREE enrichment (Fig. 7f, Marchig et al., 1982; German et al., 1993; 1999; Mills et al., 1993; Chavagnac et al., 2005). The metalliferous sediments are unlikely to have positive Ce anomalies, as long as they have a substantial hydrothermal component in them.

#### **4.2.3.1.2 Eu anomaly**

PAAS normalized REE patterns of the bulk sediments reveal another significant feature (Fig. 7g), viz., a positive Eu anomaly compared to its neighboring lanthanides. Positive Eu anomalies reflect a large hydrothermal component in the sediments which is also exhibited by hydrothermal fluids, as well as other hydrothermal phases (German et al., 1993; Mills et al., 1993; Klinkhammer et al., 1994; Mills and Elderfield, 1995; Hrischeva and Scott, 2007). Fractionation of Eu from other REEs and reduction of  $\text{Eu}^{+3}$  to  $\text{Eu}^{+2}$  can occur at temperatures above 200–250 °C (e.g., Bau, 1991). REE fractionation controlled by redox equilibrium at high temperatures can lead to LREE enrichment and positive Eu anomalies in reduced metalliferous fluids at active spreading centers (e.g., Bau, 1991). Metalliferous sediments from TAG (German et al., 1993) also have similar REE patterns with respect to LREE depletion and positive Eu anomaly. The degree of Eu anomaly is the result of mixing which indicates a small component of REE sourced from the hydrothermal fluids mixed into the major source of REE from ambient seawater (Chavagnac et al., 2005).

In order to determine whether the degree of Eu anomaly indicates the proximity to hydrothermal source, we plotted Eu/Sm ratios of our sediments along with other ridge flank sediments (Bender et al., 1971), near vent sediments (German et al., 1995, 1997, 1999) along with plume particulates (German et al., 1990, 2002; Sherrell et al., 1999) and vent fluids (Klinkhammer et al., 1994; Michard and Albarède, 1986) (Fig. 7). Eu/Sm ratios of our sediments are more similar to those of ridge flank metalliferous sediments, average plume particulates and far field plume particulates ratios (Fig. 9, and references therein).

### 4.2.3.2 Leaching Studies

#### 4.2.3.2.1 Characterizing the leach fraction

Shale normalized REE patterns of bulk, HCl leachates and residue are plotted along with data from the literature for various possible sources such as i) seawater, ii) plume particulates iii) vent fluids, iv) MORB, v) sulfides and vi) metalliferous sediments in Fig. 7. The REE concentrations and the shale normalized patterns of HCl leachates are remarkably similar to that of bulk sediments (Fig. 7g) indicating that most of the REEs in the bulk sediment are dominated by REEs in the leach fraction. Leachates seem to account for >90 % of total REEs in the sediments (Table 5) suggesting that they are oxide-bound. The REE patterns of the leachates show a positive Eu anomaly, a negative Ce anomaly and LREE depletion compared to MREE.

The negative Ce anomaly and the HREE enrichment in the sediments (both bulk and leach) are similar to seawater data, and plume particles from the EPR, TAG and Rainbow hydrothermal sites as plume particles essentially scavenge REE from ambient seawater. Negative Ce anomaly, HREE enrichment along with positive Eu anomaly is also similar to the metalliferous sediments of TAG and OBS vent field (Fig. 7). Higher REE concentration in our sediments however are probably due to the extensive scavenging of dissolved REE from seawater onto hydrothermally derived Fe–Mn oxyhydroxide colloidal particles (Barrett and Jarvis, 1988; Olivarez and Owen, 1989; German et al., 1990; Edmonds and German, 2004).

We have normalized REE to Fe in leach in our sediments and compared with that of plume particles as Fe oxides/hydroxides are the host phase in both situations. The  $REE/Fe_{(leach)}$  have been calculated and presented in Table 6. The average  $REE/Fe_{(leach)}$  in our sediments is  $0.96 \times 10^{-2}$  which is an order higher than the Fe oxy-hydroxides ( $2 \times 10^{-3}$ ) found in the Rainbow hydrothermal field, which are in turn an order higher ( $1.6 \times 10^{-4}$ ) than the ratios of plume particulates in that area (Chavagnac et al., 2005). Similarly, particulate REE/Fe ratios in neutrally buoyant plumes of TAG (German et al., 1990) are 10 fold greater than end member vent fluids. This is consistent with what is already known from the study of both plumes and ridge flank hydrothermal sediments that uptake of dissolved REE from seawater causes the REE content of Fe–oxyhydroxides material to evolve continuously with in a dispersing hydrothermal plume, leading to progressive higher REE/Fe ratios with increasing distance from the initial vent source (Mitra et al., 1994; German et al., 2002; Edmonds and German, 2004). Sherrell et al.

(1999) contend that in a time scale of plume advection, adsorption reflects near-instantaneous equilibrium of hydrothermal precipitates with ambient seawater. Earlier studies on metalliferous sediments from EPR (Ruhlin and Owen, 1986; Olivarez and Owen, 1988) and also the ancient sedimentary sequences in America (Murray et al., 1991) have suggested that the REE uptake will continue until the time of burial and the signatures acquired before burial are retained in the geological record.

It has been suggested that REE content and REE/Fe in metalliferous sediments is a function of by distance from the hydrothermal source (Ruhlin and Owen 1986; German et al., 1990). Studies showed that ridge proximal sediments have maximum values of total REE compared to sediments further from the ridge axis due to abundance of metalliferous component present in proximal sediments (Ruhlin and Owen, 1986; Olivarez and Owen, 1988; Murray et al., 1991). However, we are not able to ascertain if the variations in Fe/Mn and REE/Fe with depth in our sediments are related to the distance from the hydrothermal source or to the variation in intensity of hydrothermal activity with time. With an average spreading rate of 18 to 35 mm/yr of adjacent ridges (CIR and SEIR – Royer et al., 1989), the site would have moved a small distance of 5 to 11 km during the age span of the core (~300 kyr; see Mascarenhas-Pereira et al., 2006 and Nath et al., 2008 for age details).

#### **4.2.3.2.2 Provenance of the detrital component**

The shale normalized REE patterns for the residues shows LREE depletion, HREE enrichment and a pronounced Eu anomaly (Fig. 7g). The residue left after HCl leach would contain detrital phases like silicates, sulfides and resistant minerals (Cronan and Hodkinson, 1997). The possible aluminosilicate contribution to the CIB can come from i) terrestrial sources through turbiditic sedimentation (Kolla et al., 1976; Rao and Nath, 1988; Nath et al., 1989, 1992b; Fagel et al., 1994) ii) dust from the distal sources such as Australia or African or Indian subcontinent (e.g., Kolla and Biscaye, 1977) and iii) local mid oceanic ridge basalts (Rao and Nath, 1988; Nath et al., 1989, 1992a). Terrigenous sediments from the northern part of the CIB are characterized by flat REE patterns, without Ce fractionation (Nath et al., 1992a). The terrigenous input to the core location at 16° S in CIB would be minimal, as it was found that the influx of terrigenous sedimentation is limited to 8–10° S (Nath et al., 1989, 1992b; Fagel et al., 1994; Nath, 2001). There must therefore be an additional source contributing to the HCl-insoluble fraction.

La enrichment in combination with positive Eu anomaly (Fig. 7g) is distinctly similar to the REE patterns of vent fluids from Rainbow hydrothermal site (Fig. 7c) as well as sulfides from OBS vent field on EPR (German et al., 1999), sulfides from white and black smokers recovered from TAG (Mills and Elderfield., 1995) and west Tasmania, Australia (Fig. 7e) (Whitford et al., 1988). Similar REE patterns are a common feature in many massive sulfides associated with oceanic hydrothermal systems such as Southern Explorer Ridge (Barrett et al., 1990) and Juan de Fuca Ridge (Krasnov et al., 1994). Further, proportion of sulfides forming elements such as Fe, V, Zn and Pb (10 to 80 %) are relatively high in the HCl insoluble fraction compared to other elements such as lanthanides, Co and Ni (<9%) and suggests that a sulfidic contribution to residue is possible.

HREE fractionation over MREE in the HCl-insoluble residue suggests a contribution of MORB like source (Fig. 7d, Nath et al., 1992b). Thus, we consider that the residue contains a mixture of three components namely i) sulfide type hydrothermal material, ii) MORB derived weathered detritus and iii) clastic silicates from distal sources.

The importance of the relative proportion these potential sources contributing to the residue (i.e. terrigenous material, sulfides and MORB) is assessed by modeling the REE data using ternary mixing equations as done for major elements (Section 4.2.1.1).

$$\int_{terrigenous} + \int_{sulfides} + \int_{MORB} = 1$$

$$C_{mix}^i = (\int_{terrigenous} \times C_{terrigenous}^i) + (\int_{sulfides} \times C_{sulfides}^i) + (\int_{MORB} \times C_{MORB}^i)$$

Three end-member used here are terrigenous sediments from northern Indian Ocean, published literature on sulfides (Mills and Elderfield, 1995; German et al., 1999; Whitford et al., 1988) and MORB. The results of these calculations are presented on a shale normalized REE pattern in Fig. 10. To avoid a bias, the mixing calculations were repeated using composition of sulfides from different locations viz., TAG, EPR, and west Tasmania, Australia (Fig. 10). The results of sulfidic contribution has varied only marginally (between 64 and 72%) when any of the sulfidic end member from different areas was used. Relative proportions of terrigenous component (10–20 %), sulfides (64–72 %) and MORB (16–18 %) reproduce the REE patterns shown for the acid-insoluble residue suggesting that the terrigenous and MORB source contribution to the REEs in the residue is lower than that of sulfidic-type



material. However, these calculations should be considered as indicative and may not represent the proportion in which they are incorporated during the sediment formation (see Chavagnac et al., 2005 for discussion).

#### **4.2.4. Evidence for hydrothermal component from the presence of nontronite**

SEM–EDAX studies of some of the lithic grains recovered from the core were dense, massive and highly porous, and were similar to some of the lithic grains found in the hydrothermal system on the Juan de Fuca Ridge (Murnane and Clague, 1983). The grains contained Fe and Al (averaging 24 % Fe<sub>2</sub>O<sub>3</sub> and 14 % Al<sub>2</sub>O<sub>3</sub>) and the calculated formula (based on 24 O atoms) and the composition is close to those of ferruginous smectites (Newman, 1987; Schöps et al., 1993). The Fe<sub>2</sub>O<sub>3</sub>/SiO<sub>2</sub> ratios are close to 0.51 and fall within the previously reported values for nontronites (McMurtry et al., 1983; Murnane and Clague, 1983; Alt, 1988; Severmann et al., 2004). To identify if any ferruginous smectites of hydrothermal origin are present in the sediments studied here, infrared spectroscopy and ICP–MS analyses were carried out on the clay–sized sediment fraction (<2 µm).

IR studies show an intense SiO<sub>2</sub> stretching absorption at ~ 1020 cm<sup>-1</sup> for all the four samples studied (Fig. 11), which corresponds to a very low tetrahedral Fe<sup>3+</sup> content in the sample (e.g., Goodman et al., 1976; Cole, 1985; Schöps et al., 1993). OH bending vibration between 920 and 820 cm<sup>-1</sup> results from a variable substitution of Al by Fe. Smaller absorption bands occur at 820, ~887 and 935 cm<sup>-1</sup>, the first two bands suggesting Al–OH deformation in nontronite (Farmer and Russel, 1967), and the third band may suggest the presence of beidellite (White, 1971). The absorption band at ~880 cm<sup>-1</sup> is attributed to the substitution of octahedral Fe by Al in the smectites (Cole, 1985), or to the Fe–Al–OH substitution in ferruginous smectites (Russel, 1979) and also to the Al–OH deformation in nontronites (Frost et al., 2002, and references therein). The OH–bending vibration at 920 cm<sup>-1</sup> in this study is similar to that seen in nontronites studied by Farmer and Russell (1967).

Absorption bands are seen at 3625, 3592 and 3563 cm<sup>-1</sup> in the OH–stretching region which can represent Al–Fe–OH stretching either in ferruginous smectites (Russell, 1979) or in nontronites (Frost et al., 2002, and references therein). This equivalent band at 3564 cm<sup>-1</sup> is indicative of Fe–FeOH stretching vibration in nontronites (Van der Marcel and Beutel Spacher, 1976). IR studies, therefore, suggest that the clay sized sediments studied here contain smectites of dioctahedral series of monmorillonite–beidellite–nontronite with a dominance of nontronites and ferruginous smectites.

Occurrence of both the ferruginous smectites and the nontronitic clays in these sediments would probably suggest hydrothermal origin (e.g., McMurtry and Yeh, 1981). Iyer et al. (1997) have recovered volcanogenic–hydrothermal material (vhm), and sediments with a composition close to nontronite at 14° S and 75° 56.1' E which is ~45 km from the 76° 30' E fracture zone in the CIB and suggested that they form through submarine exhalations and deposition in the surrounding siliceous sediments. Hydrothermal nontronites commonly have very low Al content (Singer et al., 1984), while our sediments contain higher Al ( $\text{Al}_2\text{O}_3$  ~14 wt %). Nontronites characterized by distinctly elevated Al and Ti content have been described to be formed at low temperatures (32–48° C) in the Central Pacific seamounts (Schöps et al., 1993). Compositionally, bulk sediments as well as the < 2  $\mu\text{m}$  sized clay fraction studied here; fall in the field of Alvin nontronites (Fig. 12), which were calculated to form at 59+/-5° C (Severmann et al., 2004). Lack of a well crystallized iron mineral such as hematite in our samples indicates the dominance of amorphous Fe–oxides/oxyhydroxides which may form at temperatures of ~ 100° C (McMurtry and Yeh, 1981).

In summary, the leaching experiment on sediments has shown that they contain a mixture of Fe and Mn–oxides of metalliferous nature in acid–leachable fraction and sulfides in a fraction of residue in addition to the aluminosilicates from lithogenic sources. A series of deposits ranging from sulfides through iron oxides to Mn oxides with different proportions of these phases have been found in the Red Sea deposited from the same hydrothermal source (Cronan, 1976). Precipitation of sulfides during the cooling of ascending magmatic fluids on contact with seawater and fractionation of Mn and Fe on increase of pH and Eh (Krauskopf, 1957) could be a possible mechanism for the co–occurrence of Fe, Mn oxides and sulfides.

## **5. Summary**

Geochemical studies of the bulk as well as the HCl soluble fraction of sediments collected from the flanks of a seamount near the 76° 30' E fracture zone complex in the CIB indicate that the major elements have contribution from detrital sources of Bengal Fan and weathering of basinal and mid–oceanic ridge basalts on one hand and hydrothermal (mainly for Fe and Mn) and authigenic sources on the other. Shale–normalized REE patterns are indistinguishable from metalliferous sediments and plume particulates from the EPR, TAG and Rainbow hydrothermal sites. The sediments studied here are estimated to contain ~50–80 % and 90–95 % hydrothermal component in the bulk and leach fraction,

respectively. While the ternary mixing calculations on bulk sediments indicate 35–45 % metalliferous sediments could reproduce Fe and Mn values of our sediments, the HCl insoluble fraction indicate that the sulfide-like material dominates (64–72 %) over terrigenous (10–20 %) and MORB derived (16–18 %) components the residue. Occurrence of both Fe–Mn oxides and sulfides is similar to those occurring in Red Sea.

Infrared spectroscopic studies indicate the presence of a dioctahedral smectites of monmorillonite–beidellite–nontronite series, with dominance of nontronite and ferruginous smectite suggesting a hydrothermal nature. Moreover, the composition of clay sized fraction is similar to known hydrothermal nontronitic clays from the Alvin site. The temperature of formation for these smectites is estimated to range from 50 to 100° C. The presence of metalliferous sediments near the fracture zone suggests that the fracture zones may provide an easy conduit for in-situ volcanic activity in the area. While the earlier reports have shown spherules and lithic grains of metalliferous nature, this is the first study to report hydrothermal features in the bulk sediments of the CIB. The intraplate volcanoes located along the fracture zones, have therefore not only induced hydrothermal activity but also contributed nuclei and metals for the formation of the manganese nodules which are widespread in the CIB.

### **Acknowledgments**

The sampling was carried out as a part of the project “Environmental Impact Assessment of Nodule mining” funded by the Department of Ocean Development, Government of India. M.B.L would like to thank Dr Rahul Sharma for allowing to carry out this work. We thank Director, National Institute of Oceanography, India, for permitting to publish this work, Neetu Singh, M. Aparna for technical advice and help in data processing, Dr Parameswaran for his guidance during the IR studies, P. Pawaskar for all the plots, Naman, Nivedita, Vitya and Trupti for preparing the samples and analytical assistance, V. D. Khedekar for the SEM photographs and EDAX analyses C. Moraes for XRF analytical work and Drs. V. Balaram and T. G. Rao of National Geophysical Research Institute for the ICP–MS facility. G. P. Glasby has corrected an earlier version of the manuscript. This is NIO contribution number xxxx

## References

- Albarède, F., 1995. *Introduction to Geochemical Modeling*. 543 pp, Cambridge Univ. Press, New York.
- Alt, J. C., 1988. Hydrothermal oxide and nontronite deposits on seamount in the Eastern Pacific. *Mar. Geol.* 81, 227–239.
- Aoki, S., Kohyama, N., Hotta, H., 1996. Hydrothermal clay minerals found in sediment containing yellowish–brown material from the Japan Basin. *Mar. Geol.* 129, 3–4, 331–336.
- Aoki, S., Kohyama, N., Ishizuka, T., 1991. Sedimentary history and chemical characteristics of clay minerals in cores from the distal part of the Bengal Fan (ODP 116). *Mar. Geol.* 99(1-2), 175–185.
- Amakawa, H., Alibo, D. S., Nozaki, Y., 2000. Nd isotopic composition and REE pattern in the surface waters of the eastern Indian Ocean and its adjacent seas. *Geochim. Cosmochim. Acta* 64, 1715–1727.
- Bach, W., Banerjee, N. R., Dick H. J. B., Baker, E. T., 2002. Discovery of ancient and active hydrothermal systems along the ultra–slow spreading Southwest Indian Ridge 10–16E. *Geochem. Geophys. Geosys.* 3(7), doi:10.1029/2001GC000279.
- Banerjee, R., Ray, D., 2003. Metallogensis along the Indian Ocean Ridge system. *Curr. Sci.* 85(3), 321–327.
- Barrett, T. J., Jarvis, I., 1988. Rare earth element geochemistry of metalliferous sediments from DSDP Leg 92, the East Pacific Rise transect. *Chem. Geol.* 67, 243–259.
- Barrett, T. J., Taylor, P. N., Lugowski, J., 1987. Metalliferous sediments from DSDP Leg 92: the East Pacific Rise Transect. *Geochim. Cosmochim. Acta* 51, 2241–2253.
- Balaram, V., Rao, T. G., 2003. Rapid determination of REEs and other trace elements in geological samples by microwave acid digestion and ICP–MS. *At. Spectr.* 24, 206–212.
- Batiza, R., 1982. Abundance, distribution and size of volcanoes in the Pacific Ocean and implications for origin of non–hotspot volcanoes. *Earth Planet. Sci. Lett.* 60, 195–206.
- Bau, M., 1991. Rare–earth element mobility during hydrothermal and metamorphic fluid–rock interaction and the significance of the oxidation state of europium. *Chem. Geol.* 93, 219–230.
- Bender, M., Broeker, W. S., Gornitz, V., Middel, U., Day, R., Sun, S. S., Biscaye, P., 1971. Geochemistry of three cores from the East Pacific Rise. *Earth Planet. Sci. Lett.* 12, 425–433.

- Borole D. V., 1993. Deposition of Mn–Cu–Ni enriched sediments during glacial period in the Central Indian Basin. *Curr. Sci.* 65(10), 778–782.
- Boström, K., Peterson, M. N. A., 1969. The origin of aluminium–poor ferromanganoan sediments in areas of high heat flow on the East Pacific Rise. *Mar. Geol.* 7, 427–447.
- Cave, R. R., German, C. R., Thomson, J., Nesbitt, R. W., 2002. Fluxes to sediments from the Rainbow Hydrothermal plume, 36° 14' N on the MAR. *Geochim. Cosmochim. Acta* 66, 1905–1923.
- Chavagnac, V., German, C. R., Milton, J. A., Palmer, M. R., 2005. Sources of REE in sediment cores from the Rainbow vent site (36° 14' N, MAR). *Chem. Geol.* 216, 329–352.
- Cherkashev, G. A., 1992. Geochemistry of metalliferous sediments from ore–forming areas in the ocean. In: Gramberg, I. S., Ainemer, A. I. (Eds.), *Hydrothermal Sulfide Ores and Metalliferous Sediments of the Ocean*. St. Petersburg (Nedra), pp. 138–152 (in Russian).
- Clauer, N., Stille, P., Bonnot–Courtois, C., Moore, W. S., 1984. Nd–Sr isotopic and REE constraints on the genesis of hydrothermal manganese crusts in the Galapagos. *Nature* 311, 743–745.
- Cole, T. G., 1985. Composition, oxygen isotope geochemistry, and the origin of smectite in the metalliferous sediments of the Bauer Deep, southeast Pacific. *Geochim. Cosmochim. Acta* 49, 221–235.
- Cronan, D. S., 1976. Basal metalliferous sediments from the eastern Pacific. *Geol. Soc. Am. Bull.* 87, 928–934.
- Cronan, D. S., Hodkinson, R. A., 1997. Geochemistry of hydrothermal sediments from ODP Sites 834 and 835 in the Lau Basin, southwest Pacific. *Mar. Geol.* 141, 237–268.
- Das, P., Iyer, S. D., Kodagali, V. N., 2007. Morphological characteristics and emplacement mechanism of the seamounts in the Central Indian Ocean Basin. *Tectonophysics* 443, 1–18.
- Debrabant, P., Fagel, N., Chamley, H., Bout, V., Caulet, J. P., 1993. Neogene to Quaternary clay mineral fluxes in the Central Indian basin. *Palaeogeography, Palaeoclimatology, Palaeoecology* 103(3–4), 117–131
- Deer, W., Howie, R., Zussman, J., 1967. *Rock–Forming Minerals*. Pearson Education Ltd publishing. 2nd edition.
- Donnelly, T. W., 1980. Chemical composition of deep sea sediments–Sites 9 through 425, Legs 2 through 54. In: Rosendahl, B. R., Hékinian, R., et al., (Eds.), *Initial. Rep. Deep Sea Drill. Proj. 54*, Washington, D.C: Government Printing Office, 899–949.

- Douville, E., Charlou, J. L., Oelkers, E. H., Bienvenu, P., Jove Colon, C. F., Donval, J. P., Fouquet, Y., Prieur, D., Appriou, P., 2002. The Rainbow vent fluids (36° 14' N, MAR): the influence of ultramafic rocks and phase separation on trace metal content in Mid-Atlantic Ridge hydrothermal fluids. *Chem. Geol.* 184, 37–48.
- Dymond, J., 1981. Geochemistry of Nazca Plate surface sediments: an evaluation of hydrothermal, biogenic, detrital, and hydrogenous sources. In: Kulm, L. D., et al., (Eds.), *Nazca Plate: Crustal Formation and Andean Convergence*. *Geol. Soc. Am. Mem.* 154, 133–174.
- Edmonds, H. N., German, C. R., 2004. Particle geochemistry in the Rainbow hydrothermal plume, Mid-Atlantic Ridge. *Geochim. Cosmochim. Acta* 68(4), 759–772.
- El Wakeel, S. K., Riley, J. P., 1957. Determination of organic carbon in the marine muds. *J. Conseil. Int. Explor. Mer.* 22, 180–183.
- Epp, D., Smooth, N. C., 1989. Distribution of seamounts in North Atlantic. *Nature* 337, 254–257.
- Fagel, N., André, L., Debrabant P., 1997. Multiple seawater-derived geochemical signatures in Indian oceanic pelagic clays. *Geochim. Cosmochim. Acta* 61(5), 989–1008
- Fagel, N., Debrabant, P., André, L., 1994. Clay supplies in the Central Indian Basin since the Late Miocene: climatic or tectonic control. *Mar. Geol.* 122, 151–172.
- Farmer, V. C., Russell, J. D., 1967. Infra-red absorption spectrometry in clay studies. *Proc. 15<sup>th</sup> Natl. Conf. on Clays and Clay Minerals* pp. 121–142.
- Frank, M., Marbler, H., Koschinsky, A., van de Flierdt, T., Klemm, V., Gutjahr, M., Halliday, A. N., Kubik, P. W., Halbach, P., 2006. Submarine hydrothermal venting related to volcanism in the Lesser Antilles: Evidence from ferromanganese precipitates. *Geochem. Geophys. Geosyst.* 7, Q04010, doi: 10.1029/2005GC001140.
- Frost, R. L., Klopogge, J. T., Ding, Z., 2002. Near-infrared spectroscopic study of nontronites and ferruginous smectite. *Spectrochim Acta Part A*, 58, 1657–1668.
- Gallant, R. M., Von Damm, K. L., 2006. Geochemical controls on hydrothermal fluids from the Kairei and Edmond Vent Fields, 23°–25°S, Central Indian Ridge. *Geochem. Geophys. Geosyst.* 7(6), Q06018, doi:10.1029/2005GC001067.
- German, C. R., 2003. Hydrothermal activity on the eastern SWIR (50° – 70°E): Evidence from core-top geochemistry, 1887 and 1998. *Geochem. Geophys. Geosyst.* 4(7), 9102, doi: 10.1029/2003GC000522.

- German, C. R., Klinkhammer, G. P., Edmond, J. M., Mitra, A., Elderfield, H., 1990. Hydrothermal scavenging of rare earth elements in the ocean. *Nature* 345, 516–518.
- German, C. R., Higgs, N. C., Thompson, J., Mills, R., Elderfield, H., Blusztajn, J., Fleet, A. P., Bacon, M. P., 1993. A geochemical study of metalliferous sediments from the TAG hydrothermal mound, 26° 08' N, Mid Atlantic Ridge. *J. Geophys. Res.* 98, 9683–9692.
- German, C. R., Barreiro, B. A., Higgs, N. C., Nelsen, T. A., Ludford, E. M., Palmer, M. R., 1995. Seawater–metasomatism in hydrothermal sediments (Escanaba Trough, northeast Pacific). *Chem. Geol.* 1119, 175–190.
- German, C. R., Bourlés, D. L., Brown, E. T., Hergt, J., Colley, S., Higgs, N. C., Ludford, E. M., Nelsen, T. A., Feely, R. A., Raisbeck, G., Yiou, F., 1997. Hydrothermal scavenging on the Juan de Fuca Ridge:  $^{230}\text{Th}_{\text{xs}}$ ,  $^{10}\text{Be}$ , and REEs in ridge–flank sediments. *Geochim. Cosmochim. Acta* 61(19) 4067–4078.
- German, C. R., Hergt, J., Palmer, M. R., Edmond, J. M., 1999. Geochemistry of a hydrothermal sediment core from the OBS vent–field, 21° N East Pacific Rise. *Chem. Geol.* 155, 65–75.
- German, C. R., Colley, S., Palmer, M. R., Khripounoff, A., Klinkhammer, G. P., 2002. Hydrothermal plume–particle fluxes at 13°N on the East Pacific Rise. *Deep Sea Res Part I* 49, 1921–1940.
- Goodman, B. A., Russell, J. D., Fraser, A. R., Woodhams, F. W. D., 1976. A Mössbauer and IR spectroscopic study of the structure of nontronite. *Clays clay Miner.* 24, 53–59.
- Grim, R. E., 1968. *Clay Mineralogy*. McGraw–Hill, Inc., New York, 596 p.
- Gupta, S. M., 1988. Radiolarian zonation and volcanic ash layers in two Quaternary sediment cores from the central Indian Ocean basin. *J. Palaeontol. Soc. India.* 33, 59–71.
- Gurvich, E. G., Levitan, M. A., Zuzmina, T. G., 1995. Chemical composition of leg 138 sediments and history of hydrothermal activity. *Proc. Ocean Drill. Program Sci. Results* 138, 769–778.
- Hein, J., Yeh, H., Alexander, E., 1979. Origin of iron–rich montmorillonite from the manganese nodule belt of the North equatorial Pacific. *Clays Clay Miner.* 27, 185–194.
- Hékinian R., Stoffers, P., Ackermann, D., Révillon, S., Maia, M., Bohn, M., 1999. Ridge–hotspot interaction: the Pacific–Antarctic ridge and the foundation seamounts. *Mar. Geol.* 160, 199–223.
- Hodkinson, R. A., Cronan, D. S., 1991. Regional and depth variability in the composition of cobalt–rich ferromanganese crusts from the SOPAC area and adjacent parts of the central equatorial Pacific. *Mar Geol.* 98, 437–44.

- Hodkinson, R. A., Stoffers, P., Scholten, J., Cronan, D. S., Jeschke, G., Rogers, T. D. S., 1994. Geochemistry of hydrothermal manganese deposits from the Pitcairn Island hotspot, southeastern Pacific. *Geochim. Cosmochim. Acta* 58, 5011–5029.
- Hrischeva, E., Scott, S. D., 2007. Geochemistry and morphology of metalliferous sediments and oxyhydroxides from the Endeavour segment, Juan de Fuca Ridge. *Geochim. Cosmochim. Acta* 71, 3476–3497.
- Iyer, S. D., 2005. Evidences for incipient hydrothermal event(s) in the Central Indian Basin: A review. *Acta Geol. Sin.* 79, 77–86.
- Iyer, S. D., Sudhakar, M., 1993. A new report on the occurrence of zeolitites in the abyssal depth of the Central Indian Ocean Basin. *Sediment. Geol.* 84, 169–178.
- Iyer, S. D., Prasad, S. M., Gupta, S. M., Charan, S. N., 1997. Evidence for recent hydrothermal activity in the Central Indian Ocean Basin. *Deep Sea Res.* 44, 1167–1184.
- Iyer, S. D., Mascarenhas-Pereira, M. B. L., Nath, B. N., 2007. Native aluminium (spherules and particles) in the Central Indian Basin sediments: Implications on the occurrence of hydrothermal events. *Mar. Geol.* 240, 177–184.
- James, R. H., Elderfield, H., Palmer, M. R., 1995. The chemistry of hydrothermal fluids from the Broken Spur site, 29° N Mid-Atlantic Ridge. *Geochim. Cosmochim. Acta* 59, 651–659.
- Jarvis, I., 1985. Geochemistry and origin of Eocene–Oligocene metalliferous sediments from the central equatorial Pacific: Deep Sea Drilling Project sites 573 and 574. In: Mayer, L., Theyer, F., et al., (Eds.), Initial. Rep. Deep Sea Drill. Proj. vol. 85, Washington, D.C: U. S. Government Printing Office; 781–804.
- Kamesh Raju, K. A., 1993. Magnetic lineation, fracture zones and seamounts in the Central Indian Ocean Basin. *Mar. Geol.* 109, 195–201.
- Kamesh Raju, K. A., Ramprasad, T., 1989. Magnetic lineation in the Central Indian Basin for the period A24–A21: A study in relation to the Indian Ocean Triple Junction. *Earth Planet. Sci. Lett.* 95, 395–402.
- Karisiddaiah, S. M., Iyer, S. D., 1992. A note on incipient spilitisation of Central Indian Basin basalts. *J. Palaeontol. Soc. India* 39, 518–523.
- Kastner, M., 1979. Zeolites. In: Burns, R. G., (Eds.), *Marine Minerals. Reviews in mineralogy.* vol. 6, Mineralogical Society of America, Washington, DC. pp 111–122.



- Karl, D. M., McMurtry, G. M., Malahoff, A., Garcia, M. O., 1988. Loihi Seamount Hawaii: A mid-plate volcano with a distinctive hydrothermal system. *Nature* 335, 532–535.
- Klinkhammer, G. P., Elderfield, H., Edmonds, J. M., Mitra, A., 1994. Geochemical implications of rare earth element patterns in hydrothermal fluids from mid-ocean ridges. *Geochim. Cosmochim. Acta* 58, 5105–5113.
- Kolla, V., Biscaye, P. E., 1977. Distribution and Origin of Quartz in the Sediments of the Indian Ocean. *Journal of Sedimentary Research* 47, 642–649.
- Kolla, V., Henderson, L., Biscaye P. E., 1976. Clay mineralogy and sedimentation in the western Indian ocean. *Deep Sea Research and Oceanographic Abstracts* 23, 949–961.
- Krauskopf, K. B., 1957. Separation of manganese from iron in sedimentary processes. *Geochim. Cosmochim. Acta* 12, 61–84.
- Kryc, K. A., Murray, R. W., Murray, D. W., 2003. Elemental fractionation of Si, Al, Ti, Fe, Ca, Mn, P, and Ba in five marine sedimentary reference materials: Results from sequential extractions. *Anal. Chim. Acta* 487(1), 117–128.
- Kurian, S., Nath, B. N., Ramaswamy, V., Naman, D., Rao, T. G., KameshRaju, K. A., Selvaraj, K., Chen, C. T. A., 2008. Possible detrital, diagenetic and hydrothermal sources for Holocene sediments of the Andaman backarc basin. *Mar. Geol.* 247, 178–193.
- Li, Y. H., 2000. *A Compendium of Geochemistry: from Solar Nebula to the Human Brain*. Princeton Uni. Press, Princeton, NJ.
- Lisitzin, A. P., Crook, K. A. W., Bogdanov, Yu. A., Zonenshain, L. P., Murav'ev, K. G., Tufar, W., Gurvich, E. G., Gordeev, V. V., Ivanov, G. V., 1992. Hydrothermal fields of the Manus basin rift zone. *Int. Geol. Rev.* 35, 105–126.
- Ludford, E. M., Palmer, M. R., German, C. R., Klinkhammer, G. P., 1996. The geochemistry of Atlantic hydrothermal particles. *Geophys. Res. Lett.* 23(23), 3503–3506.
- Marchig, V., Gundlach, H., Möller, P., Schley, F., 1982. Some geochemical indicators for discrimination between diagenetic and hydrothermal metalliferous sediments. *Mar. Geol.* 50, 241–256.
- Mascarenhas-Pereira, M. B. L., Nath, B. N., Borole, D. V., Gupta, S. M., 2006. Nature, source and composition of volcanic ash in sediments from a fracture zone trace of Rodriguez Triple Junction in the Central Indian Basin. *Mar. Geol.* 229, 79–90.

- McLennan, S. M., 1989. Rare earth elements in sedimentary rocks: Influence of provenance and sedimentary processes. In: Lipin, B. R., Mckay, G. A. (Eds.), *Geochemistry and Mineralogy of the Rare Earth Elements*. vol. 21, *Rev. Mineral.* pp. 169–200.
- McMurtry, G. M., Yeh, H. –W., 1981. Hydrothermal clay mineral formation of East Pacific Rise Bauer Basin sediments. *Chem. Geol.* 32, 189–205.
- McMurtry, G. M., de Carlo, E. H., Kim, K. H., 1991. Accumulation rates, chemical partitioning, and Q-mode factor analysis of metalliferous sediments from the North Fiji Basin. *Mar. Geol.* 98, 271–295.
- McMurtry, G. M., Wang, C. –H., Yeh, H. –W., 1983. Chemical and isotopic investigations into the origin of clay minerals from the Galapagos hydrothermal mound field. *Geochim. Cosmochim. Acta* 47, 475–489.
- Michard, A., Albarède, F., 1986. The REE content of some hydrothermal fluids. *Chem. Geol.* 55, 51–60.
- Mills, R. A., Elderfield, H., 1995. Rare earth element geochemistry of hydrothermal deposits from the active TAG Mound, 26°N Mid–Atlantic Ridge. *Geochim. Cosmochim. Acta* 59, 3511–3524.
- Mills, R. A., Elderfield, H., Thomson, J., 1993. A dual origin for the hydrothermal component in a metalliferous sediment core from the Mid–Atlantic Ridge. *J. Geophys. Res.* 98, 9671–9678.
- Mills, R. A., Wells, D. M., Roberts, S., 2001. Genesis of ferromanganese crusts from the TAG hydrothermal field. *Chem. Geol.* 176, 283–293.
- Mitra, A., Elderfield, H., Greaves, M. J., 1994. Rare earth elements in submarine hydrothermal fluids and plumes from the Mid–Atlantic Ridge. *Mar. Chem.* 46, 217–235.
- Mukhopadhyay, R., Batiza, R., 1994. Basinal seamounts and seamount chains of the Central Indian Ocean: Probable near–axis origin from a fast–spreading ridge. *Mar. Geophys. Res.* 16(4), 303–314.
- Münch, U., Lalou, C., Halbach, P., Fujimoto, H., 2001. Relict hydrothermal events along the super–slow Southwest Indian spreading ridge near 63°56'E–mineralogy, chemistry and chronology of sulfide samples. *Chem. Geol.* 177, 3–4, 341–349.
- Murnane, R., Clague, D. A., 1983. Nontronite from a low temperature hydrothermal system on the Juan de Fuca Ridge. *Earth Planet. Sci. Lett.* 65, 343–352.
- Murray, R. W., Buchholtz Ten Brink, M. R., Gerlach, D. C., Russ III, G. P., Jones, D. L., 1991. Rare earth, major, and trace elements in chert from the Franciscan Complex and Monterey Group,

- California: Assessing REE sources to fine-grained marine sediments. *Geochim.Cosmochim. Acta* 55, 1875–1895.
- Nath, B. N., 1993. Rare earth element geochemistry of the sediments, ferromanganese nodule and crusts from the Indian Ocean. Ph.D. thesis. Goa Uni., India.
- Nath, B. N., 2001. Geochemistry of sediments. In: Sen Gupta, R., Desa, E. (Eds.), *The Indian Ocean: A perspective*. vol. 2, New Delhi, India: Oxford & IBH; 645–689.
- Nath, B. N., Rao, B. R., 1998. Late Pliocene–Pleistocene sedimentation and episodic volcanism recorded by a sediment core of the central Indian Basin, paper presented at 6<sup>th</sup> International Conference on Palaeoceanography, Lisbon, Portugal.
- Nath, B. N., Balaram, V., Sudhakar, M., Plüger, W. L., 1992a. Rare earth element geochemistry of the ferromanganese deposits from the Indian Ocean. *Mar. Chem.* 38, 185–208.
- Nath, B. N., Bau, M., Rao, B. R., Rao, Ch. M., 1997b. Trace and rare earth elemental variation in Arabian Sea sediments through a transect across the oxygen minimum zone. *Geochim. Cosmochim. Acta* 61, 2375–2388.
- Nath, B. N., Roelandts, I., Sudhakar, M., Plüger, W. L., 1992b. Rare earth element patterns of the Central Indian Basin sediments related to their lithology. *Geophys. Res. Lett.* 19(12), 1197–1200.
- Nath, B. N., Roelandts, I., Sudhakar, M., Plüger, W. L., Balaram, V., 1994. Cerium anomaly variation in ferromanganese nodules and crusts from the Indian Ocean. *Mar. Geol.* 120, 385–400.
- Nath, B. N., Borole, D. V., Aldahan, A., Patil, S. K., Mascarenhas–Pereira, M. B. L., Possnert, G., Ericsson, T., Ramaswamy, V., Gupta, S. M., 2008. <sup>210</sup>Pb, <sup>230</sup>Th, and <sup>10</sup>Be in Central Indian Basin seamount sediments: Signatures of degassing and hydrothermal alteration of recent origin. *Geophys. Res. Lett.* 35, L09603, doi:10.1029/2008GL033849.
- Nath, B. N., Rao, V. P. C., Becker, K. P., 1989. Geochemical evidence of terrigenous influence in deep-sea sediments up to 8° S in the Central Indian Basin. *Mar. Geol.* 87, 301–313.
- Nath, B. N., Plüger, W. L., Roelandts, I., 1997a. Geochemical constraints on the hydrothermal origin of ferromanganese encrustations from the Rodriguez Triple Junction, Indian Ocean. In: Nicholson, K., Hein, J. R., Bühn, B., Dasgupta, S. (Eds.), *Manganese Mineralization: Geochemistry and Mineralogy of Terrestrial and marine Deposits*. vol. 119, Geol. Soc. Spec. Publ. pp. 192–221.
- Newman, A. C. D., 1987. *Chemistry of clays and clay minerals*. Longman Scientific and Technical, Harlow.

- Olivarez, A. M., Owen, R. M., 1989. REE/Fe variation in hydrothermal sediments: implication for the REE content of seawater. *Geochim. Cosmochim. Acta* 53, 757–762.
- Owen, R. M., Olivarez, A. M., 1988. Geochemistry of rare earth elements in pacific hydrothermal sediments. *Mar. Chem.* 25(2), 183–196.
- Plüger, W. L., Friedrich, G., Stoffers, P., 1985. Environmental controls on the formation of deep-sea ferromanganese concretions: Monograph Series on Mineral Deposits. 25, 31–52.
- Plüger, W., Schwarz, P., Scholten, J., Stoffers, P., 1986. Geochemie und Mineralogie der Sedimente des Mittelindischen Rückens zwischen 21°S und der Rodriguez Triple Junction (SO 43)., In: GEMINO 2: Geothermale Metallogenie Indischer Ozean., 1–38, Aachen, RWTH, Aachen.
- Rao V. P., Nath, B. N., 1988. Nature, distribution and origin of clay minerals in grain size fractions of sediments from manganese nodule field, Central Indian Ocean Basin. *Indian J. Mar. Sci.* 17, 202–207.
- Ruhlin, D. E., Owen, R. M., 1986. The rare earth element geochemistry of hydrothermal sediments from the East Pacific Rise: Examination of a seawater scavenging mechanism. *Geochim. Cosmochim. Acta* 50, 393–400.
- Russell, J. D., 1979. An Infrared spectroscopic study of the interaction of nontronite and ferruginous montmorillonite with alkali metal hydroxides. *Clay Miner.* 14, 127.
- Schöps, D., Herzig, P. M., Halbach, P., Friedrich, G., Blum, N., 1993. Mineralogy, chemistry and oxygen isotope thermometry of nontronitic smectites from Central Pacific seamounts. *Chem. Geol.* 106, 331–343.
- Severmann, S., Mills, R. A., Palmer, M. R., Fallick, A. E., 2004. The origin of clay minerals in active and relict hydrothermal deposits. *Geochim. Cosmochim. Acta* 68(1), 73–88.
- Sherrell, R. M., Field, M. P., Ravizza, G., 1999. Uptake and fractionation of rare earth elements on hydrothermal plume particles at 9° 45' N, East Pacific Rise. *Geochim. Cosmochim. Acta* 52, 669–677.
- Sholkovitz, E. R., 1989. Artifacts associated with the chemical leaching of sediments for rare-earth elements. *Chem. Geol.* 77, 47–51.
- Singer, A., Stoffers, P., Heller-Kallai, I., Szafrank, D., 1984. Nontronite in a deep-sea core from the south Pacific. *Clays clay Miner.* 32, 375–383.

- Staudigel, H., Hart, S. R., Koppers, A. A. P., Constable, C., Workman, R., Kurz, M., Baker, E. T., 2004. Hydrothermal venting at Vailulu'u Seamount: The smoking end of the Samoan chain. *Geochem. Geophys. Geosyst.* 5, Q02003, doi:10.1029/2003GC000626.
- Sukumaran, N. P., Banerjee, R., Borole, D. V., Gupta, S. M., 1999. Some aspects of volcanic ash layers in the Central Indian Basin. *Geo-Mar. Lett.* 18, 203–208.
- Sun, S. S., Nesbitt, R. W., Sharaskin, A. Y., 1979. Geochemical characteristics of mid-ocean ridge basalts. *Earth Planet Sci. Lett.* 44(119), 138.
- Taylor, S. R., McLennan, S. M., 1985. *The Continental Crust: Its Composition and Evolution.* 312 pp., Blackwell, Malden, Mass.
- Toth, J. R., 1980. Deposition of submarine crusts rich in manganese and iron. *Geol. Soc. Am. Bull.* 91, 44–54.
- Van der Marcel, H. W., Beutel Spacher, H., 1976. *Atlas of the infrared spectra of clay minerals and their admixtures.* pp. 146–148, Elsevier, Amsterdam.
- Walter, P., Stoffers, P., 1985. Chemical characteristics of metalliferous sediments from eight areas on the Galapagos rift and East Pacific Rise between 2° N and 42° S. *Mar. Geol.* 65, 271–287.
- White, J. L., 1971. Interpretation of infrared spectra of soil minerals. *Soil Sci.* 112, 22–31.
- Ziegler, C. L., Murray, R. W., Hovan, S. A., Rea, D. K., 2007. Resolving eolian, volcanogenic, and authigenic components in pelagic sediment from the Pacific Ocean. *Earth Planet. Sci. Lett.* 254, 3–4, 416–432

## Figure captions

**Fig. 1.** Sampling location of sediment core AAS 61/BC 8 (shown as a star). a) Sampled area in the Central Indian Basin (CIB) with reference to India and shows the sediment distribution (numbers correspond to sediment types shown in the legend) (adopted from Nath et al., 1992b); b) detailed tectonic map showing the fracture zones, ridge axis and location of seamounts (shown as dots). Sampled location falls close to the cluster of seamounts in the vicinity of fracture zone (base map from Kamesh Raju, 1993) and c) 3-dimensional topographic map (bathymetry data set ETOPO 5 (National Geophysical Data Centre (NGDC) 1988). As seen in figures b) and c), the sample location falls on the flank of a seamount.

**Fig. 2.** Discriminating source using composition of sediments. a)  $\text{Fe}_2\text{O}_3$  versus  $\text{Al}_2\text{O}_3$  plot and b)  $\text{Al}_2\text{O}_3$  % versus  $\text{K}_2\text{O}$ . The plots illustrate that the bulk sediments are a mixture of variable proportions of Fe-rich and Al-rich end members. References of literature data are given in the text.

**Fig. 3.**  $\text{K}_2\text{O}-\text{Al}_2\text{O}_3-(\text{CaO}+\text{Na}_2\text{O})$  diagram shows mixing between zeolite, plagioclase and Fe-smectites on one side and illite, Al-rich beidellite, micaceous clays from Bengal Fan, kaolinite and chlorite on other. Residue exhibits reduction of Ca and Na and compositional similarity with micaceous clays and smectites of Bengal Fan and illites.

**Fig. 4.** Fe/Mn ratio of AAS 61/BC 8 is compared with metalliferous sediments from ridge flank as well as near field sediments along with plume particulates. (The literature data for Fe/Mn ratios is taken from Gurvich et al., 1995; Donnelly, 1980; Jarvis 1985; Lisitzin et al., 1992; Cherkashev, 1992; Li, 2000; Cronan, 1976; German et al., 1993, 1995, 1997, 1999; Barrett et al., 1987; Hodkinson and Cronan, 1991; James et al., 1995; Boström and Peterson, 1969; Sherrell et al., 1999; Ludford et al., 1996 and Mitra et al., 1994). Fe/Mn ratios in our sediments are similar to those of ridge flank metalliferous sediments. Conversely, the near field metalliferous sediments and plume particulates have higher Fe/Mn ratios compared to the ridge flank metalliferous sediments.

**Fig. 5.** Ternary plot of Al-Fe-Mn illustrating the compositional similarity of bulk sediments to Bauer deep metalliferous sediments. Compositional fields of CIB (Borole, 1993), Pacific and EPR sediments (Plüger et al., 1985 and references therein) along with mean composition of 3 major sediment types in CIB (Nath et al., 1989) are shown.

**Fig. 6.** Co/Zn versus Cu+Ni+Co content (Toth, 1980, modified by Nath et al., 1997a). While the data for all bulk sediments fall in the hydrothermal field, leach data for only unit 2 sediments show hydrothermal signatures. Consistent with their pelagic nature, unit 1 sediments fall away from hydrothermal field.

**Fig. 7.** Shale normalized REE distribution patterns for bulk, HCl leachates and residue of AAS 61/BC 8 are shown along with a) seawater (Eastern Indian Ocean-Amakawa et al., 2000); b) plume particulates (Rainbow-Edmonds and German, 2004; TAG-German et al., 1990 and EPR-Sherrell et al., 1999), c) vent fluid (EPR-Klinkhammer et al., 1994; MAR-German et al., 1990; Rainbow hydrothermal site-

Douville et al., 2002); d) Indian Ocean MORB–Nath et al., 1992b; e) sulfides (TAG–Mills and Elderfield, 1995; OBS vent site at 21° N on EPR–German et al., 1999; West Tasmania, Australia–Whitford et al., 1988) and f) metalliferous sediments–German et al., 1993; 1999; Chavagnac et al., 2005 and Mills et al., 1993. While the patterns for bulk as well as leach closely resemble the plume particulate data, those for residue seem to be a contribution from OBS type sulfides and MORB.

**Fig. 8.** A plot of  $\Sigma$ REE versus Cu+Ni+Co content (both for bulk and leach) in comparison with literature data for hydrothermal deposits and metalliferous deposits (Clauer et al., 1984, modified by Nath et al., 1997a).

**Fig. 9.** PAAS normalized Eu/Sm ratios of our sediments are compared with metalliferous sediments from ridge flank as well as near field sediments along with plume particulates and vent fluids. The data is from Jarvis et al. (1985); Bender et al. (1971); German et al. (1990, 1995, 1997, 1999, 2002); Klinkhammer et al. (1994) and Sherrell et al. (1999).

**Fig. 10.** Ternary REE mixing calculation using 3 end members (Terrigenous sediments in the CIB; sulfides and Indian Ocean MORB) (References for these values are given in text) are presented in PAAS normalized REE patterns for the residue fractions. Relative contribution to the sulfides in the residue was estimated using sulfides from 3 different areas a) EPR (OBS); b-e) TAG (white smoker, black smoker, talus and mound); f) massive sulfides from west Tasmania, Australia. Calculations with varying sulfides have yielded nearly similar contribution (64–72%) of sulfides to residues.

**Fig. 11.** Infrared spectra of 4 sediment sections (untreated, 2  $\mu$ m size fractions). Left: OH–stretching region at 3700–3000  $\text{cm}^{-1}$  with absorption bands representing ferruginous smectite and nontronite. Right: Si–O stretching region with absorption band at 1020  $\text{cm}^{-1}$  corresponding to low Fe content in tetrahedral position of smectite. Absorption bands between 920–820  $\text{cm}^{-1}$  represent increasing Fe content in octahedral sites and the presence of nontronite, ferruginous smectite and beidellite.

**Fig. 12.** Chondrite normalized Yb/Gd vs. Eu/Eu\* in the bulk and <2  $\mu$ m sized sediments compared to the composition of nontronites and other hydrothermal precipitates from various areas (modified from Severmann et al. 2004). Samples from this study plot in the Alvin nontronite field.

Table 1. Major and rare earth element concentrations in bulk sediments of AAS 61/8.  
(All values in ppm)

Element	←----- Depth (cm) -----→									
	0-2	2-4	4-6	6-8	8-10	10-12	12-14	14-16	16-18	18-20
Al (%)	6.43	6.75	6.74	6.82	6.74	6.65	6.61	6.74	6.55	6.63
Mn (%)	1.47	1.47	1.32	1.39	1.45	1.46	1.33	1.31	1.32	1.39
Fe (%)	6.58	7.13	6.20	7.36	8.46	8.26	8.22	8.16	8.14	8.32
V	152	164	125	163	221	221	222	234	231	230
Cr	26	28	29	27	26	25	25	25	25	27
Co	138	147	140	146	149	148	139	137	139	146
Ni	782	761	562	562	490	428	333	300	294	336
Cu	473	452	378	359	332	307	279	264	258	260
Zn	177	178	171	175	184	180	176	185	197	194
Sr	187	195	179	200	224	228	231	233	234	233
Y	257	241	198	221	218	201	191	184	182	192
Zr	281	307	265	322	377	370	384	388	408	399
Ba	732	693	712	598	507	470	480	463	469	525
La	113	121	100	117	123	117	113	110	110	115
Ce	158	169	163	170	177	178	171	168	172	172
Pr	27.15	28.43	24.75	27.26	26.41	25.46	24.29	23.21	22.97	24.18
Nd	121	128	112	123	119	114	108	104	101	107
Sm	29.84	31.22	28.28	29.73	26.88	25.87	24.46	23.17	22.63	24.24
Eu	7.16	7.33	6.71	7.19	6.27	5.84	5.81	5.46	5.42	5.73
Gd	25.70	27.25	23.87	25.69	23.80	22.58	21.92	20.77	20.44	21.80
Tb	5.25	5.50	4.86	5.23	4.75	4.44	4.35	4.11	4.01	4.34
Dy	32.62	33.97	29.54	32.18	29.56	28.20	26.79	25.62	25.35	27.11
Ho	7.03	7.62	6.33	7.00	6.59	6.25	5.93	5.78	5.75	6.17
Er	20.23	22.00	18.02	20.29	19.33	18.41	17.38	16.79	16.87	17.69
Tm	3.06	3.27	2.68	3.02	2.91	2.71	2.64	2.51	2.55	2.64
Yb	17.99	19.24	16.09	17.89	17.41	16.18	15.57	14.83	14.83	15.69
Lu	2.87	3.10	2.58	2.78	2.75	2.58	2.45	2.40	2.33	2.49
Hf	6.65	7.08	6.30	7.71	8.60	8.63	8.79	8.67	8.85	8.37
Pb	19.22	19.82	19.27	19.22	19.05	18.39	18.11	17.78	17.59	17.69
Th	15.79	15.89	18.14	15.95	13.55	13.49	13.28	12.52	12.76	12.79
U	2.27	2.52	2.28	2.67	3.21	3.35	3.34	3.16	3.11	3.27



Table 2: Major element content in (wt %) bulk and leach residues

Sample (sediment depth)	Residue <sup>1</sup> %		SiO <sub>2</sub>	Al <sub>2</sub> O <sub>3</sub>	TiO <sub>2</sub>	Fe <sub>2</sub> O <sub>3</sub>	MnO	MgO	CaO	Na <sub>2</sub> O	K <sub>2</sub> O	P <sub>2</sub> O <sub>5</sub>
AAS 61/8												
4-6 cm	74	Bulk	42.26	12.87	0.61	9.97	5.905	3.07	1.98	1.63	2.54	0.91
		Residue <sup>2</sup>	59.83	12.46	0.75	5.78	0.046	1.44	0.42	0.68	2.09	0.12
8-10 cm	69	Bulk	43.86	13.96	0.73	11.95	2.345	2.81	2.22	1.37	2.85	1.16
		Residue <sup>2</sup>	57.84	12.48	0.87	6.37	0.035	1.45	0.49	0.78	2.22	0.14
12-14 cm	70	Bulk	46.55	14.13	0.77	11.06	2.168	2.73	2.16	1.32	2.87	1.02
		Residue <sup>2</sup>	57.97	12.05	0.95	6.63	0.041	1.47	0.54	0.76	2.03	0.15
18-20 cm	58	Bulk	42.14	13.84	1.05	13.57	2.316	2.64	2.43	1.75	2.86	1.24
		Residue <sup>2</sup>	55.83	12.81	1.05	6.88	0.025	1.57	0.59	0.78	2.16	0.12
MAG - 1												
80	80	Bulk	50.78	16.07	0.72	7.29	0.1	3.09	1.42	3.81	3.70	0.16
		Certified value	50.40	16.40	0.75	6.80	0.098	3.00	1.37	3.83	3.55	0.16
		Residue <sup>2</sup>	62.34	16.07	0.78	2.74	0.012	1.11	0.44	1.25	3.52	0.07

<sup>1</sup> Residue left on leaching with hot 50% HCl

<sup>2</sup> The elemental concentrations are not weight corrected

Table. 3. Analytical results (in duplicate) of USGS geochemical standard MAG\_1. (All values in ppm)

Element	Certified values			This work mean of 2 analysis			Accuracy (%)	Precision %
		±			±		(±)	(±)
Al (%)	8.66	±	0.16	8.29	±	0.15	4.28	3.7
Mn (%)	0.076	±	0.005	0.076	±	0.0004	0.51	1.03
Fe (%)	4.58	±	0.42	4.81	±	0.01	4.89	0.29
V	140	±	6	136	±	0.37	2.68	0.54
Cr	97	±	8	94.56	±	0.14	2.52	0.31
Co	20	±	1.6	20.18	±	0.03	1.06	0.29
Ni	53	±	8	52.63	±	0.06	0.71	0.23
Cu	30	±	3	29.95	±	0.001	0.17	0.01
Zn	130	±	6	130	±	1.3	0.36	2.01
Sr	150	±	15	145	±	0.8	3.61	1.11
Y	28	±	3	27.81	±	0.21	0.67	1.52
Zr	130	±	6	125	±	0.17	3.96	0.27
Ba	480	±	41	473	±	2.88	1.43	1.22
La	43	±		41.14	±	0.33	4.33	1.62
Ce	88	±	9	84.81	±	0.31	3.62	0.74
Pr	9.3	±		9.02	±	0.03	3.04	0.71
Nd	38	±	5	37.1	±	0.2	2.36	1.09
Sm	7.5	±	0.6	7.81	±	0.09	4.13	2.43
Eu	1.5	±	0.14	1.52	±	0.02	1.37	2.17
Gd	5.8	±	0.7	5.68	±	0.06	2.1	2.01
Tb	0.96	±	0.09	0.97	±	0.002	1.2	0.31
Dy	5.2	±	0.3	5.19	±	0.11	0.19	4.39
Ho	1.02	±	0.1	1.03	±	0.02	0.78	4.67
Er	3	±		2.94	±	0.01	2.08	0.58
Tm	0.43	±		0.43	±	0.01	0.35	4.9
Yb	2.6	±	0.3	2.61	±	0.01	0.31	0.69
Lu	0.4	±	0.04	0.39	±	0.01	1.5	4.06
Hf	3.7	±	0.5	3.81	±	0.06	2.91	3.13
Pb	24	±	3	24.05	±	0.17	0.21	1.44
Th	11.9	±	1	12.25	±	0.28	2.98	4.51
U	2.7	±	0.3	2.83	±	0.07	4.78	4.81

Table 4: Comparative data results from leaching experiment of MAG-1 ( $\mu\text{mol/gm}$ )

	<b>Si</b>	<b>Al</b>	<b>Ti</b>	<b>Fe</b>	<b>Mn</b>	<b>Ca</b>
<b>This study</b>						
residue	8330	2521	78	274	1.35	65.6
Bulk	8477	3149	89.4	910	14.08	263
Certified <sup>a</sup>	8414	3215	94	849	14	254
% element in residue	99	78	83	32	10	26
<b>Kryc et al. (2003)</b>						
residue	NM	2311	70.9	443	4.3	49.7
Bulk	138	2893	78.7	849	11.8	252
Certified <sup>b</sup>	8381	3212	94	852	13.8	244
% element in residue		72	75	52	31	20

<sup>a</sup> source USGS website ([http://minerals.cr.usgs.gov/geo\\_chem\\_stand/marine.html](http://minerals.cr.usgs.gov/geo_chem_stand/marine.html))

<sup>b</sup> As mentioned in Kryc et al. (2003).

Table 5: Relative proportion in HCl leachates and residue fraction in AAS 61/BC 8. (All values in %)

Sample ID:	4-6 cm		8-10 cm		12-14 cm		18-20 cm	
Analyte (%)	residue	leach	residue	leach	residue	leach	residue	leach
Al	66	34	59	41	59	41	57	43
Fe	15	85	13	87	13	87	14	86
V	19	81	14	86	15	85	10	90
Cr	55	45	58	42	45	55	43	57
Co	3	97	3	97	2	98	3	97
Ni	7	93	7	93	8	92	9	91
Cu	8	92	7	93	7	93	6	94
Zn	71	29	80	20	31	69	56	44
Sr	27	73	27	73	24	77	39	61
Y	4	96	4	96	5	95	3	97
La	8	92	8	92	9	91	6	94
Ce	9	91	8	92	7	93	7	93
Pr	6	94	7	93	8	92	5	95
Nd	5	95	6	94	7	93	5	95
Sm	4	96	5	95	7	93	4	96
Eu	5	95	7	93	7	93	6	94
Gd	4	96	4	96	5	95	4	96
Tb	4	96	4	96	6	94	3	97
Dy	4	96	5	96	6	94	4	96
Ho	4	96	4	96	6	94	4	96
Er	4	96	5	95	6	94	4	96
Tm	5	95	5	95	7	93	5	95
Yb	6	94	6	94	8	92	5	95
Lu	6	94	6	94	8	92	5	95
Pb	23	77	25	75	15	85	22	78
Th	34	66	25	75	30	70	19	81
U	38	62	28	72	24	76	26	74

Table. 6. Important elemental ratios of the sediments of AAS 61/ BC 8

Depth (cms)	0-2	2-4	4-6	6-8	8-10	10-12	12-14	14-16	16-18	18-20
<b>Ratios</b>										
Co+Ni+Cu (ppm)	1393	1360	1080	1068	971	882	751	701	690	743
Co/Zn	0.78	0.83	0.82	0.83	0.81	0.82	0.79	0.74	0.7	0.76
∑REE (ppm)	572	607	539	588	585	567	543	526	527	546
Eu/Eu*	1.22	1.18	1.22	1.22	1.17	1.14	1.18	1.17	1.19	1.17
Ce/Ce*	0.66	0.66	0.75	0.7	0.71	0.75	0.76	0.77	0.79	0.75
(La/Yb) <sub>P<sub>AAS</sub></sub>	0.46	0.47	0.46	0.48	0.52	0.53	0.53	0.55	0.55	0.54
Fe/Mn	4.47	4.85	4.71	5.31	5.84	5.67	6.17	6.23	6.18	6
Fe <sub>2</sub> O <sub>3</sub> /Al <sub>2</sub> O <sub>3</sub>	0.78	0.8	0.7	0.82	0.95	0.94	0.94	0.92	0.94	0.95
∑REE/Fe	0.0087	0.0085	0.0087	0.008	0.0069	0.0069	0.0065	0.0061	0.0056	0.0052
MSI*	44.38	43.97	47.25	43.81	40.5	40.64	40.9	41.58	40.92	40.58
∑REE/Fe(leach)	na	129.5	na	86	na	86	na	na	na	93

Na: not analyzed

\* Metalliferous sediment index

Table. 7. Fe normalized element concentrations of the bulk sediments of this study compared with literature data.

Element	This study	CIR basalts <sup>a</sup>	RTJ sediments (cfb) <sup>b</sup>	CIR sediments <sup>c</sup>	EPR 10° S Fe-Mn oxides <sup>d</sup>	Fe oxides <sup>e</sup>	TAG nontronite <sup>f</sup>
Mn/Fe	0.1829	0.04	0.077	0.107	0.22	0.15	no data
Zn/Fe	0.0024	0.001	0.001	0.002	0.003	0.002	0.004

<sup>a</sup> Halbach, 1994

<sup>b</sup> RTJ sediments (Kuhn et al., 2000).

<sup>c</sup> CIR sediments containing 48.5 % hydrothermal Fe–Mn oxides from 21° 34' S (Plüger et al., 1986)

<sup>d</sup> East Pacific Rise (10° S) sediments mainly consisting of Fe–Mn oxides (Walter and Stoffers, 1985)

<sup>e</sup> Hydrothermal Fe oxides from the North Fiji basin (McMurtry et al., 1991)

<sup>f</sup> Hydrothermal clays from TAG zone associated with sulphide debris and Fe oxides (Severmann et al., 2004)

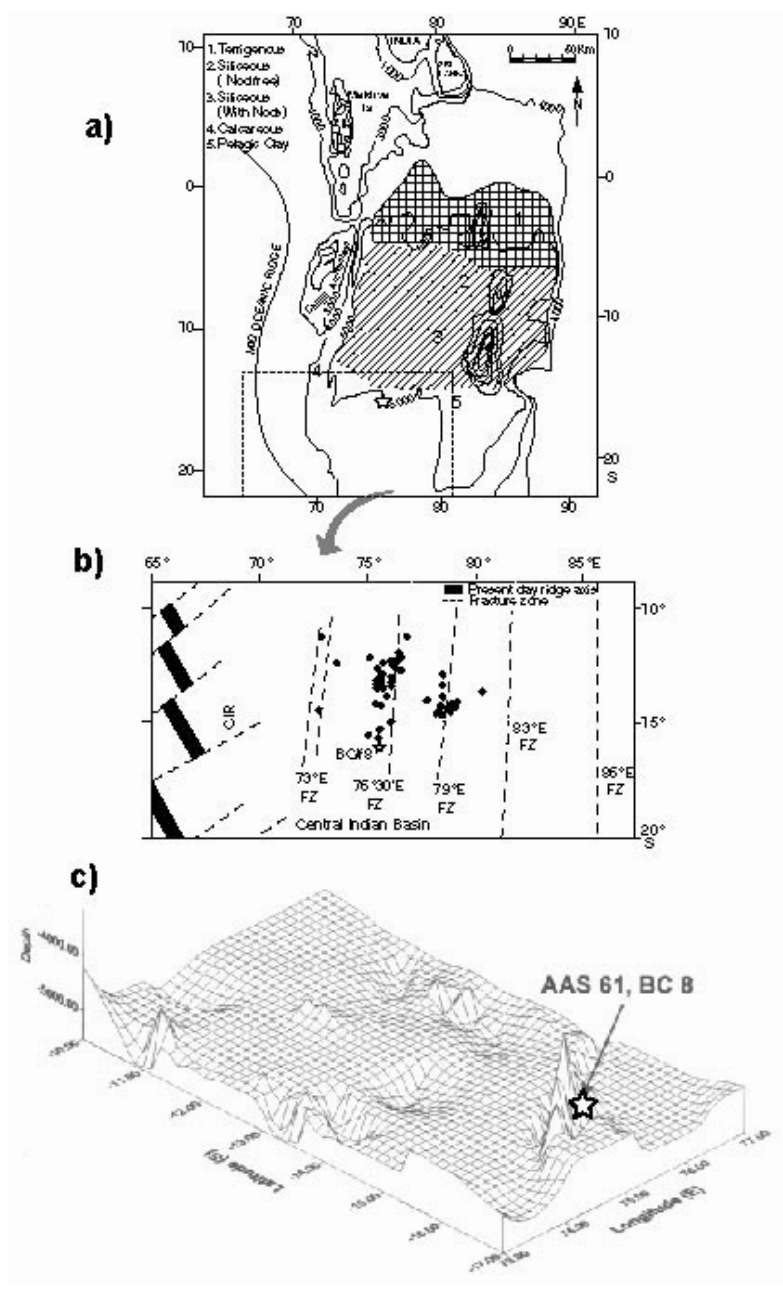


Figure 1

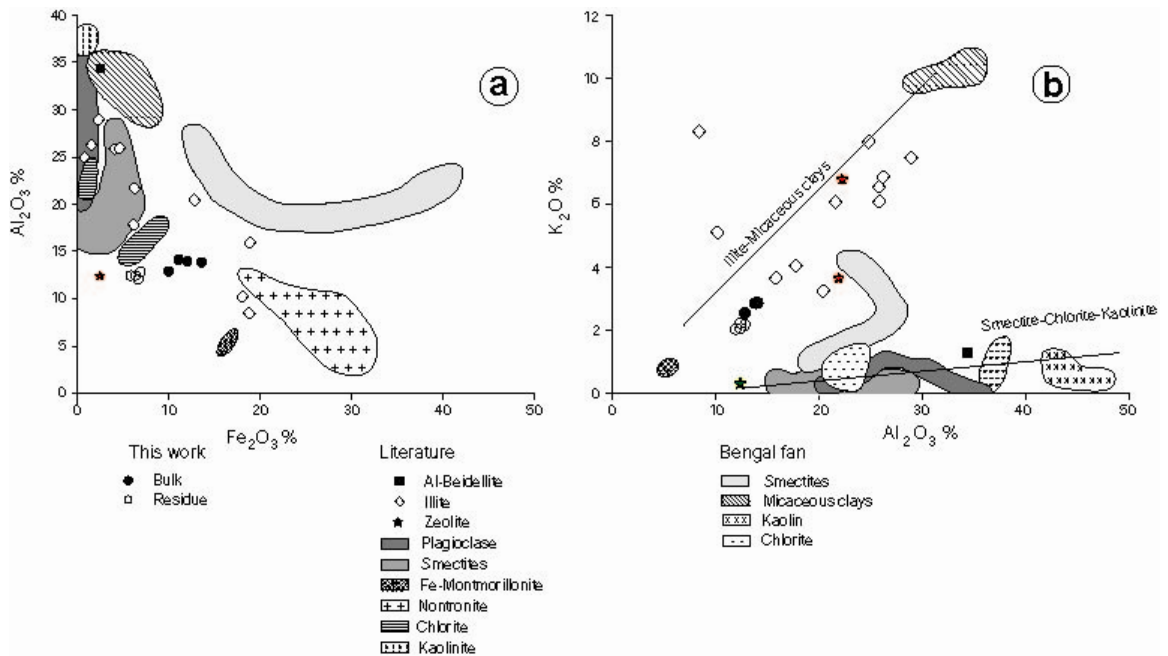


Figure 2



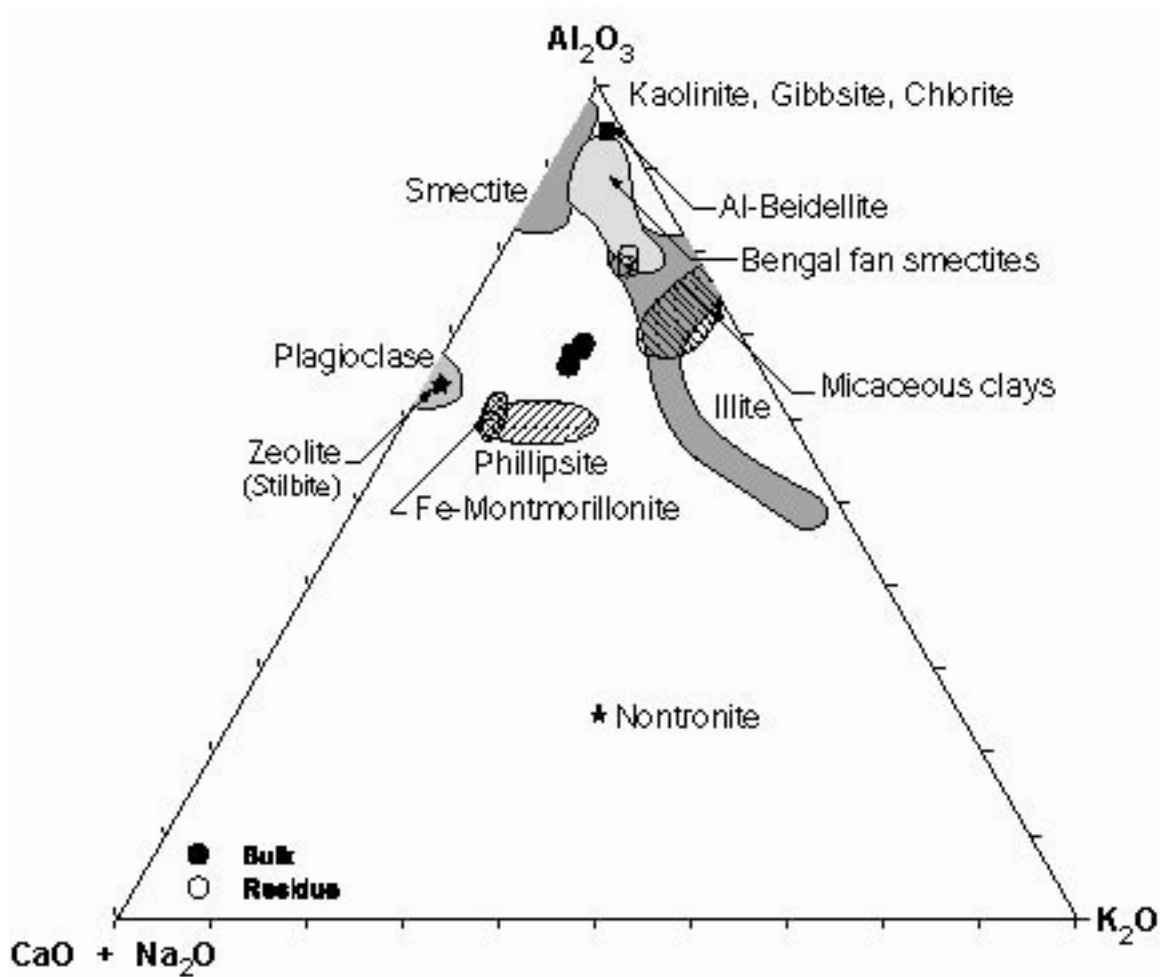


Figure 3

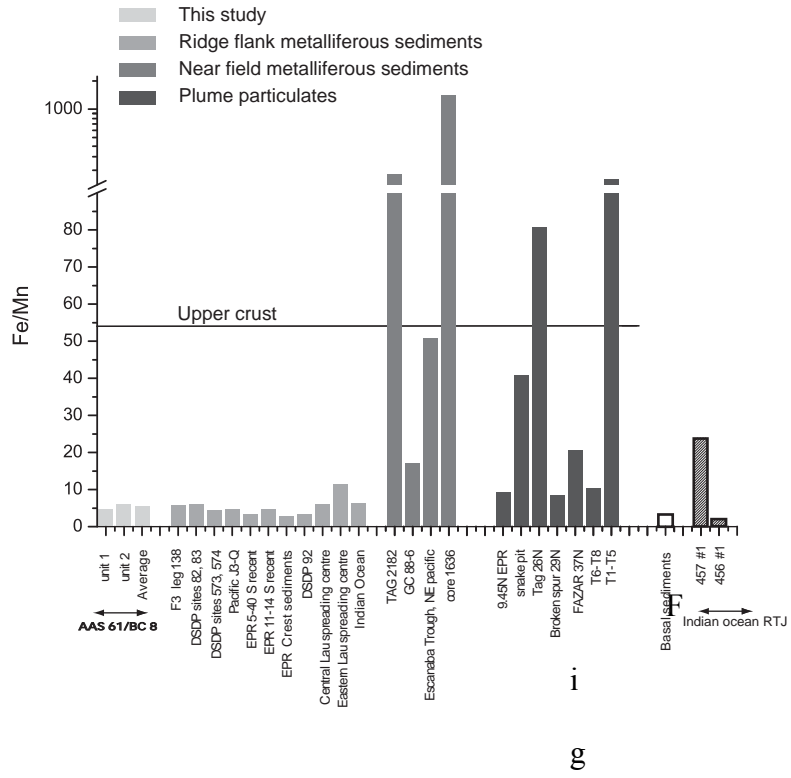


Figure 4

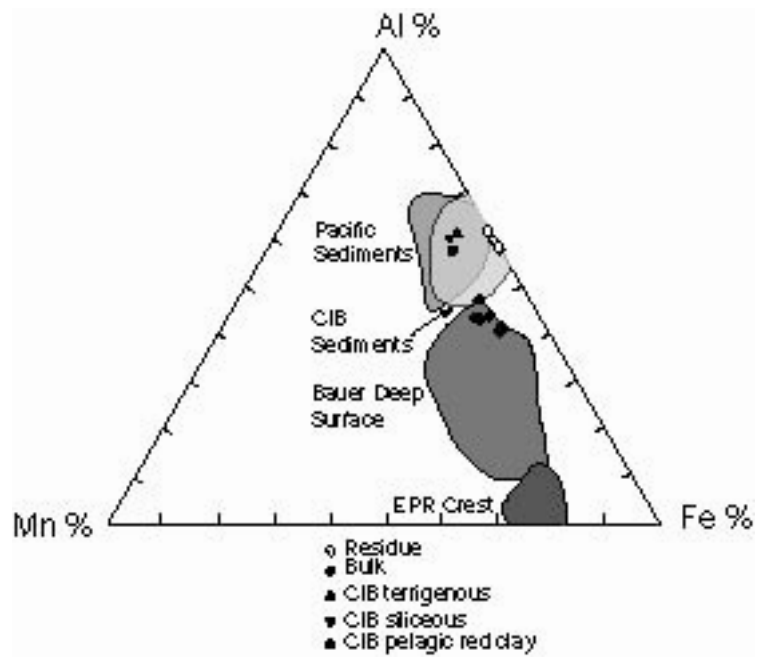


Figure 5

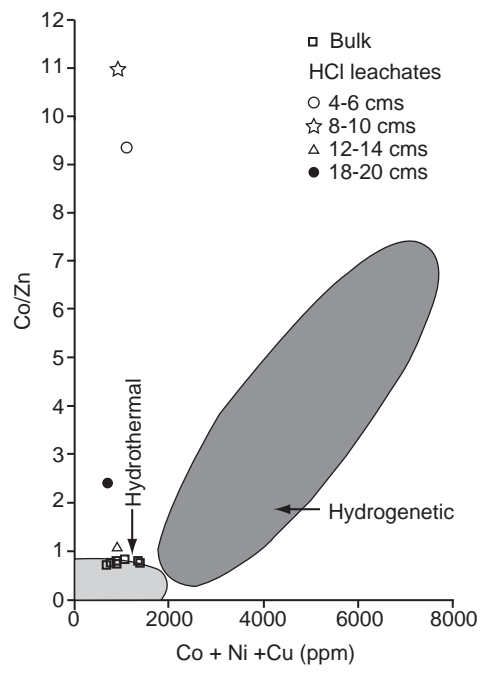


Figure 6

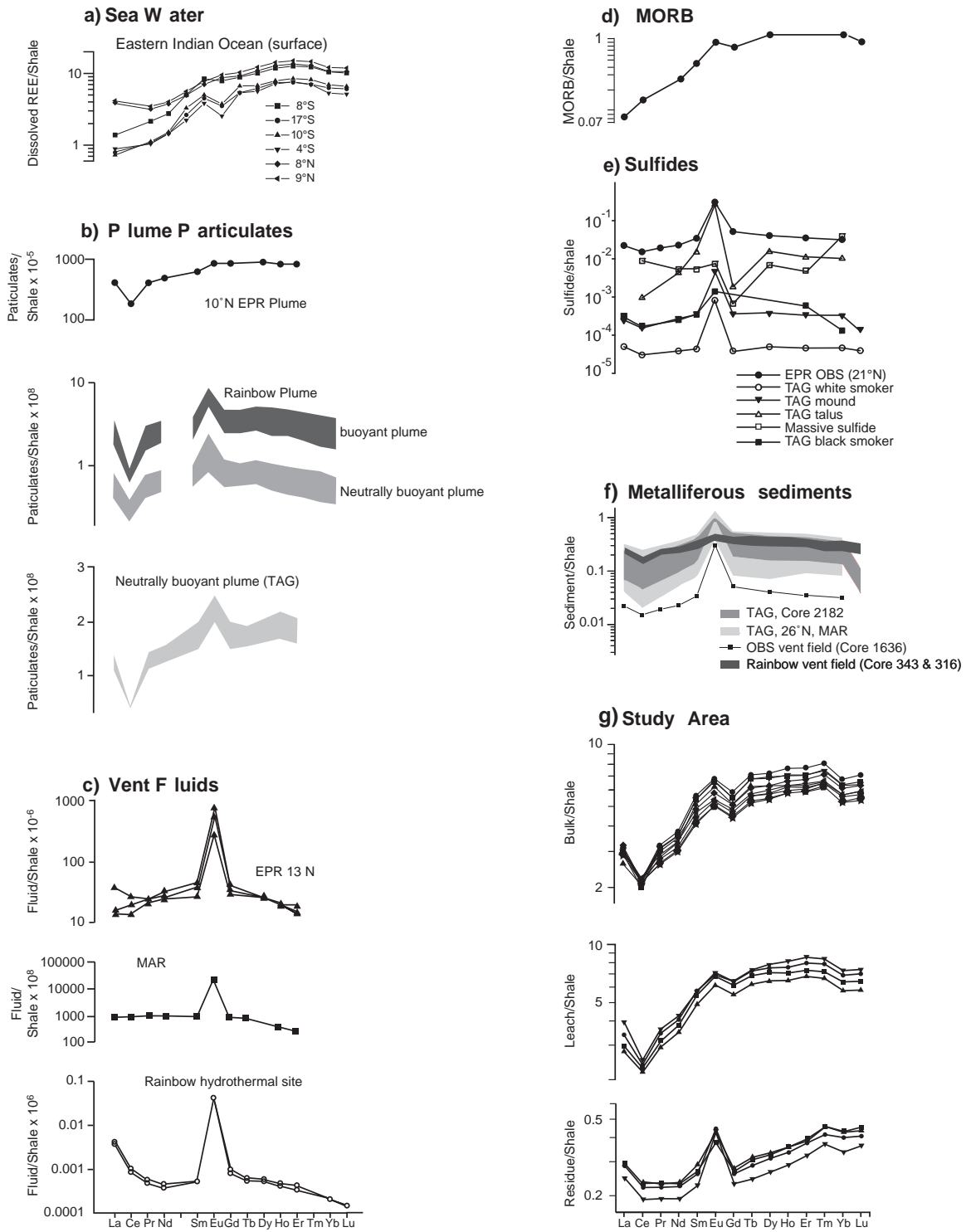


Figure 7

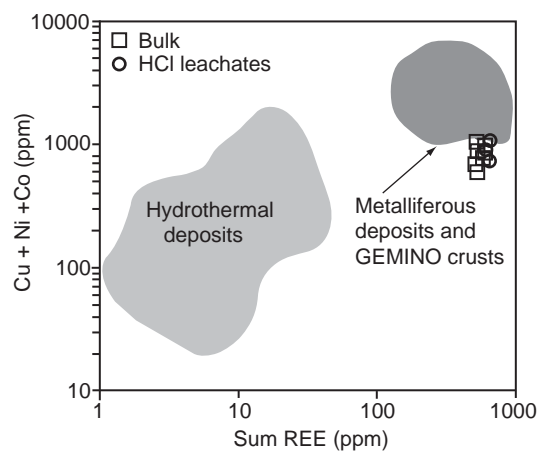


Figure 8

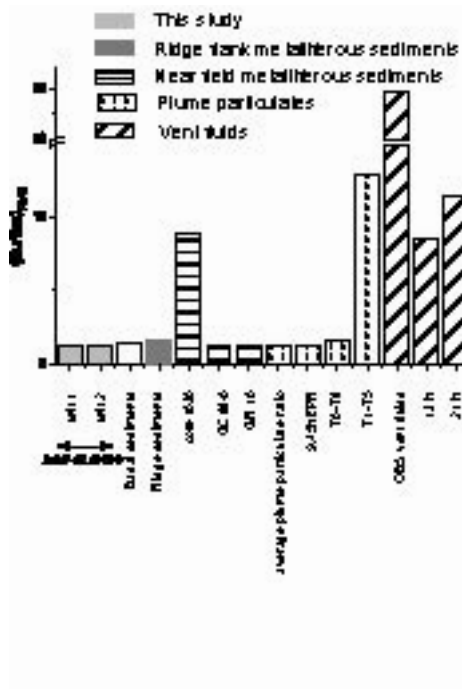


Figure 9

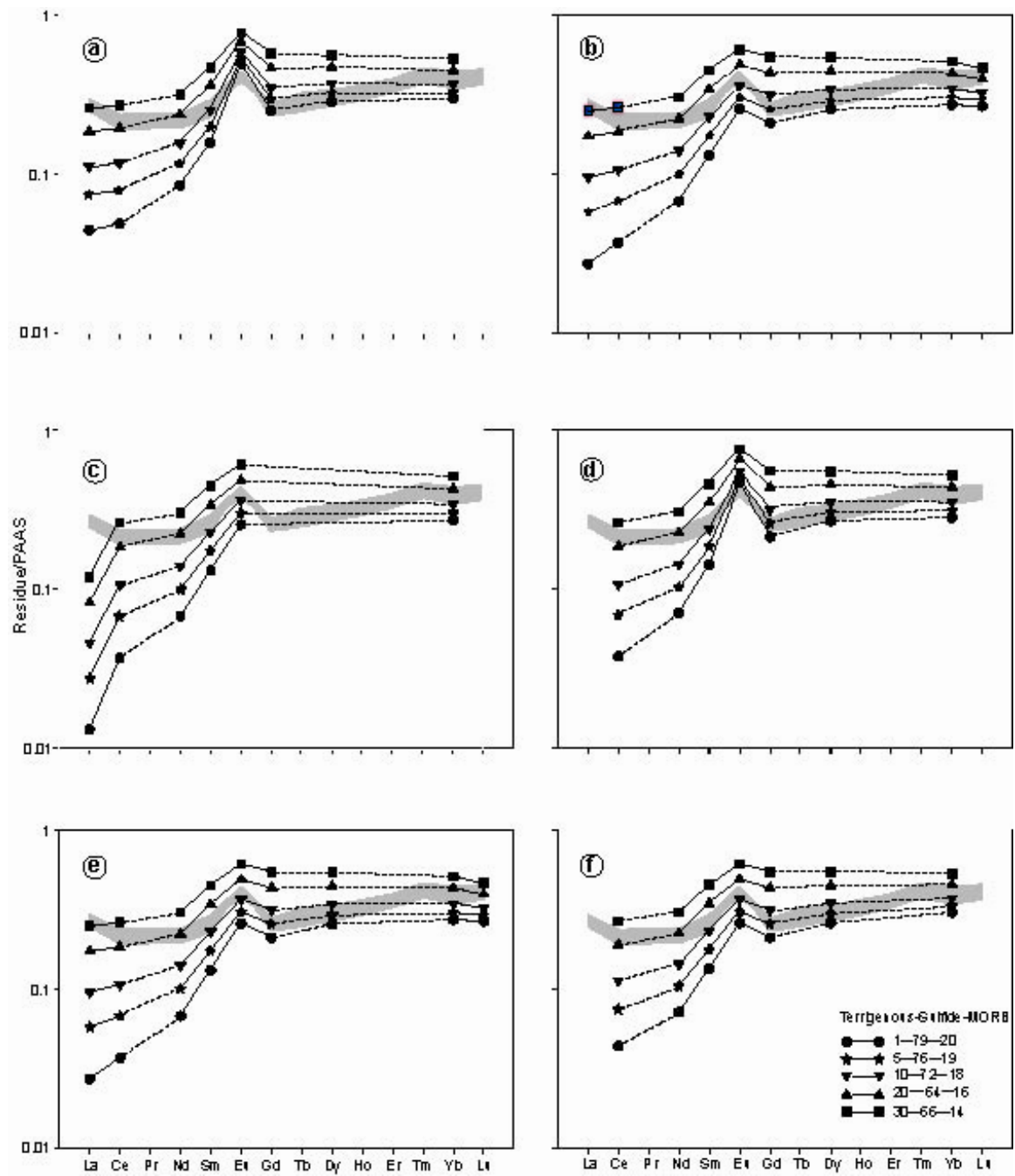


Figure 10





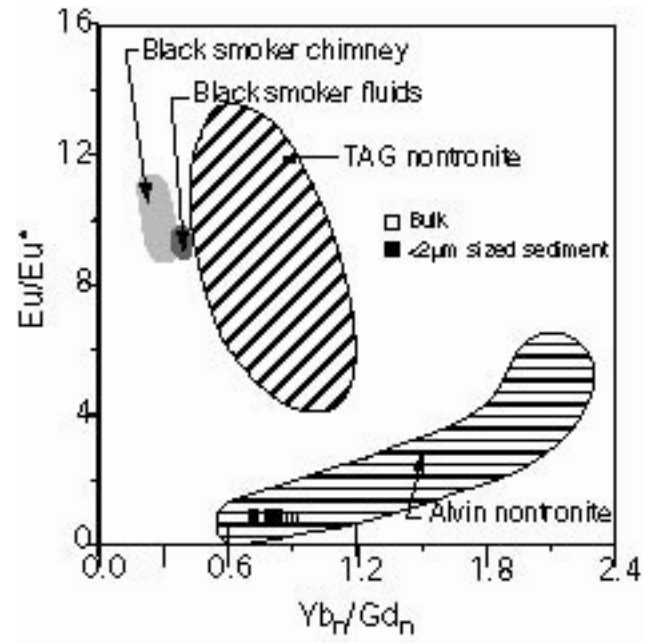


Figure 12